GROWTH KINETICS OF DISPERSED THORIA IN NICKEL BASED ALLOYS

* * *

A THESIS

presented for the

degree of

DOCTOR OF PHILOSOPHY

by

Peter Kenneth Footner

* * *

Department of Metallurgy,
Royal School of Mines,
Imperial College of Science & Technology

September, 1970

ABSTRACT

At high temperatures, nickel which contains a dispersion of thoria, shows a decrease in strength due to the increase in size of the thoria particles with time. The present research has been carried out in order to study the growth of these particles under various conditions.

The growth rate of ThO_2 particles has been measured using transmission electron microscopy for samples heated at 1350°C. under oxygen partial pressures of 10^{-8}atm., 10^{-14}atm. and 10^{-18}atm. for times up to 400 hours.

The solubilities and diffusion coefficients of thorium in nickel - chromium alloys (from 0 to 20% Cr) have been measured at 1350°C. under an oxygen partial pressure of 10^{-18}atm.

The effect of the addition of 10% platinum to a Ni - 10% Cr alloy on the diffusion coefficient and solubility of Th has been studied and the interfacial energy between a Ni - Cr - Pt alloy and ThO_2 has been measured using a sessile drop technique.

It was found that the growth of the thoria particles under the conditions mentioned was Th diffusion controlled and the growth rate was described by the Lifshitz-Wagner equation. The effect of increasing chromium content in nickel on the diffusion coefficient of thorium was to double the value for pure nickel at 20% Cr. Also it was found that there was little effect on the thorium solubility due to the presence of chromium in nickel under reducing conditions.

The addition of 10% platinum to a Ni - 10% Cr alloy was found to have increased by a factor of 50% the expected growth rate of thoria particles in this alloy.

CONTENTS

CHAPTER 1

INTRODUCTION

1.1 Dispersed Phase Materials

In recent years great interest has been shown in metals and alloys which contain a dispersion of a second phase, usually an inert oxide[1-11]. The reason for the development of these materials lies in the enhanced mechanical properties they display at high temperatures[12-19]. It has been shown by a number of workers that these materials show less decrease in rupture stress with increasing temperature than conventional alloys,[12,16,17,19] and also the presence of a dispersion of inert second phase particles tends to inhibit re-crystallisation[13, 20-22].

In order to achieve the enhanced properties mentioned above it is found essential to have an extremely small dispersoid with high thermodynamic stability. A number of different combinations of metals or alloys and oxides have been studied by other workers the most common being:-

Ni/Al_2O_3 [10,11] Ni/ThO_2 [9,12,14,21]

Al/Al_2O_3 [19,20] Cu/SiO_2 [13] $NiAl/Al_2O_3$ [8]

It was the object of this research to study the stability of the dispersoid in Ni/ThO_2 and Ni alloy/ThO_2.

1.2 Hardening Mechanism in Dispersed Phase Materials

The mechanism of hardening can be explained in terms of the interaction between the inert dispersoid and the dislocations present in the material. During any deformation or re-crystallisation the process by which atomic re-arrangement, and consequent decrease in internal energy, is achieved, is the movement of defects mainly dislocations, though the material. In dispersed phase materials there are a number of small particles present which, because this oxide dispersion is brittle compared to the ductile matrix and has a different atomic arrangement, impede the movement of the dislocations through the material. The stress necessary for the deformation of the material is therefore related to the stress required to bow the dislocation between two particles. It follows that, as long as the dispersoid is large enough to interact with the dislocations, the more finely dispersed they are the greater the increase in high temperature strength. Also it follows that the existing grain

structure of the matrix material is 'frozen in' due to the dispersoid inhibiting the nucleation of new grains and dislocation movement. This has the effect of delaying re-crystallisation until near the melting point of the material.

Once again the degree of inhibition of re-crystallisation depends on the fineness of the dispersoid. However, as there must exist a range of sizes of particles they will have differing equilibrium concentrations of the dispersoid components at the interface between the particle and the matrix. Hence, as there exists a concentration gradient between particles of differing sizes, the total interfacial energy can therefore be decreased by the growth of the larger particles at the expence of the smaller particles.

This work has been carried out in order to study the growth rates of ThO_2 in Ni and Ni/Cr alloys and the relationship between the results obtained and the theory of particle coarsening .

1.3. The Theory of Growth Rates of Second Phase Dispersions

The mathematical analysis of growth rates are based on the mass balance between growing and shrinking particles. This is expressed in terms of Fick's 1st. law

and the concentration gradients existing between two particles of differing radii. The rate of change of particle size can be controlled by either of the following steps:-

1. Diffusion through the matrix
2. The dissolution OR:
3. Deposition at the interface
4. Transfer of dispersoid material across the interface.

One such analysis by Greenwood[23] shows that for a diffusion controlled process the mean radius cubed is proportional to time of heat treatment. Lifshitz and Slyozov[24] have also considered a growth-shrinkage process controlled by the diffusion of one of the dispersoid components and the resultant equation is similar to that proposed earlier by Wagner for the same conditions. Interface contrclled conditions have been the starting criteria for theories proposed by Wagner[25] and Heckel[26]. The common starting point for all these theories is the Gibb-Thompson equation namely:-

$$\text{Ln} \quad \frac{Cr}{C\infty} = \frac{2\,V_m}{RT\,r}\,\delta$$

Where $C\infty$ = the concentration of solute at a plane interface.

C_r = the concentration of solute at the surface of a particle of radius r

r = the particle radius

V_m = the molar volume of the dispersoid

R = the gas constant

T = the temperature of the system

δ = the interfacial energy between the dispersoid and the matrix.

This formulates the variation of the interfacial solubility with radius. For diffusion controlled growth (i.e. equilibrium between the matrix and the dispersoid) we can derive an expression for the rate of change of radius of the particle i.e.:-

$$\dot{r} = \frac{-D\ V_m(Cr - C)}{r}$$

Where:-

$\dot{r}$ = the rate of increase or decrease of radius with time.

D = the diffusion coefficient of the slowest moving component of the dispersoid in the matrix.

Cr = the concentration of this component at the interface.

C = the concentration of this component at a distance far removed from the particle.

r = the radius of the particle.

The combination of these two equations with the statistical analysis of the contributions due to particles of differing radii, leads to a final growth rate equation.

Wagners[25] equation of the growth of a precipitate in fluid matrix gives:-

$$\bar{r}^3 - \bar{r}_o^3 = \frac{8\ D\ Co\ V_m^2\ \gamma\ .\ t}{9\ R\ T}$$

Where:-

$\bar{r}$ = the radius of the particles after a time t.

$\bar{r}_0$ = the radius of the particle initially

Co = the equilibrium concentration of the slowest moving species of the components of the dispersoid, at a plane interface.

t = the time of heat treatment.

All the other symbols have the same meaning as before.

The above equation was chosen for use in this work in view of its mathematical simplicity and the fact that the radius measured (the arithmetic mean) was easily determinable. The use of an equation for the growth of ThO_2 in Ni based on diffusion control is made in the light of previous studies made by other workers on oxide and non-oxide dispersion, (see section 1.4), it being

hoped that it would be possible to justify this assumption with the results of this work.

Brown [27] showed that the diffusion of Th through Ni was much slower than that of oxygen and the activation energies were:-

Th diffusion in Ni, activation energy = 178 K cal/mole

O diffusion in Ni, activation energy = 50 K cal/mole

Comparing these very high values to the energies involved in dissolution and recombination at the Ni/ThO_2 interface

$$Th \rightarrow [Th]_{Ni} = +78 \text{ K cal/mole}$$

$$O_2 \rightarrow 2[O]_{Ni} = +85 \text{ K cal/mole}$$

it would appear that the growth process should be diffusion controlled.

1.4 Literature on Growth Processes and their Application to Specific Systems

The growth of dispersoids and precipitates in various metal matrices has been of interest to a number of workers over the past ten to fifteen years, and studies have been carried out, using the theories outlined in Section 1.3

Livington [28] has studied the precipitation of a Co rich phase from copper alloys and his results indicate an increase in size of particle proportional to the cube root of treatment time in accordance with diffusion

controlled kinetics.

Heckel and De Gregorio[29] studied the coarsening of cementite in a ferrite matrix and measured the growth-shrinkage process over various time intervals. They found that the growth process was interface controlled after comparison of the results with the theory previously expounded by Heckel[26].

In a study of growth of manganese precipitates in a binary magnesium alloy A. F. Smith[30] was unable to decide conclusively the process which controlled the growth, that is, if it was interface or diffusion controlled. Smith also studied the growth of U Al_2 in uranium and concluded that the mechanism was diffusion controlled from the consideration of the activation energies[31]. The rate of coarsening of Cu in an alpha-iron matrix has been studied by Spiech and Oriani[32] and they concluded that the kinetics of ripening of the Cu precipitate in alpha-iron obeys the t to the 1/3rd power law deduced by Liftshitz[24] and Wagner[25], so that the matrix diffusion of the precipitate component controls the process. However, due to the non-sphericity of the particles, they found it necessary to modify the Liftshitz-Wagner equation both for the geometry of the

diffusion field and for the re-formulation of the Gibbs-Thompson equation.

Ardell and Nicholson[33] measured the growth rates of the gamma prime in Ni-Al alloys, and their results show good agreement with the Lifshitz-Wagner theory.

All the above reference concerned studies on growth rates of metallic or inter-metallic precipitates in metallic matrices. However, when we turn to the growth of oxide dispersions, it is evident that all previous work has been concerned with qualitative measurements. Simms[34] found that there was little change in dispersoid distribution in Thoria dispersed Nickel (T.D. Nickel) after two thousand hours at 1100°C., this he felt was due to the high stability of the Thoria particles. Doble and Quigg[35] found some coarsening of Thoria particles in T.D. Nickel, after one hour at 1370°C. in air, but the coarsening was not apparent after one hour at 1350°C. Murphy and Grant[36] found that oxide agglomeration had taken place more rapidly in samples of T.D. Nickel , undergoing creep tests at 1100°C. in air, than those tested at 1350°C. in argon under no strain. Grimwade and Jackson[37] found a fall off in tensile properties for copper containing MgO at

1000°C., and nickel containing alumina at 1300°C., and this was associated with a growth of oxide dispersion.

Tracy and Worn[38] found that treatment for sixteen hours at 1200°C., resulted in the spheriodization of the Thoria particles in T.D. Nickel, but there was no evidence of particle growth, also a single sample heated for 16 hours at 1400°C. in hydrogen showed no growth. Gatti[39] found catostrophic growth of the alumina in iron at 1400°C., under hydrogen, but the measured variations of particle size versus treatment time shows a cubic dependance as expected from the Lifshitz/Wagner diffusion controlled growth; unfortunately, these workers only measured the activation energy and a complete analysis of the growth process is difficult.

Lewis Sebohm and Martin[40] state that after annealing for 20 hours in hydrogen at 1000°C BeO particles in a Cu matrix exhibit growth, but no quantitative measurements were made.

Feisel and Cochardt[41] in their comparison of dispersion and precipitative strengthened Ni based alloys state that after 16 hours at 1177°C. alumina particles showed a slight enlargement, but no actual sizes were measured.

Inman and Smith[42] found that after annealing T.D. Nickel for 200 hours in high purity oxygen, about 10% of the ThO_2 particles had shown growth whilst the remainder was unaltered. However, this sample had oxidised and could possibly be a surface effect.

Komatsu and Grant [43] studied the stability of Silica and Alumina in Cu and they found that the particle sizes of the oxide dispersoid increased with annealing temperature and time, and that the rate is apparently effected by the dislocation density.

Dromsky Lenel and Ansell[44] measured the growth rate of alumina in Ni and the range (1170°C - 1355°C) and calculated an activation energy for the process. They found a cube relationship between particle size and time, but their analysis of the growth mechanism was incomplete, so the controlling step could not be characterised.

Sergeenkova and Berzutskii [45] studied the growth rates of various oxides in Ni and they found that the stability of the oxide was inversly proportional to their reactivity. They found the relationship between the mean radius and treatment time was a fourth power one, which is in disagreement with all theories, but

their analysis of growth rates was restricted to activation energies and hence the validity of their results is subject to question.

The same authors also measured the effects of Ti on a Ni-Al_2O_3 system and found that this decreased the growth rate, the reason they cite being a reduction in the interfacial energy between the Ni and Alumina.

As can be seen from the above literature survey the growth of inter-metallics in metallic matrices is well characterised and the observed growth rates agreed well with the Lifshitz-Wagner theory. However, analysis of growth of oxide dispersions has not received the same detailed attention, and consequently, there appears to be no complete study of the parameters that comprise the Lifshitz-Wagner growth equation.

It was the object of this research to study all the factors concerned in the growth of ThO_2 in Ni and Ni alloys.

1.5. Use of Particle Coarsening Theory to ThO_2 Dispersions in Ni and Ni Cr.

If a theory based on diffusion control is assumed for the growth of thoria in nickel and nickel alloys

one of the factors which affects the growth rate is the value of Co(the solubility of the slowest dispersoid species at a plane interface). However, considering the equation:-

$$ThO_2 \longrightarrow [Th]_{Ni} + 2[O]_{Ni}$$

assuming equilibrium at the interface we can derive a constant equal to:-

$$\gamma^2_{[O]} X^2_{[O]} \gamma_{[Th]} X_{[Th]}$$

where X represents the concentration of the species in the matrix and γ_1 activity coefficient in the system.

Consequently, as the PO_2 of the furnace gas used for growth rate treatment can be controlled, the amount of oxygen in the matrix can be fixed. As can be seen an increase in dissolved oxygen in the matrix will decrease the thorium content and consequently, alter the value of the solubility to be used in the growth equation.

It was found by Brown that the diffusion coefficient of Th in Ni was dependant on the PO_2 of the treatment gas, the value of the diffusion coefficient decreasing with decreasing PO_2 , this was thought to be due to interaction between the inter-stitial O^{2-} ions and the Th.

These two considerations mean that in order to study growth rates of thoria in nickel, the oxygen partial pressure under which heat treatment is carried out must be measured.

Owing to the poor oxidation resistance of pure Ni at high temperatures interest has been shown in ThO_2 dispersoid strengthed alloys based on a Ni-Cr matrix.

The Cr imparts good oxidation resistance to this alloy, but the effect on the growth rate had not been completely characterised. As the free energy of formation of Cr_2O_3 is a much larger negative value than that for the formation of NiO, it was expected that some of the oxygen in the lattice would become associated with the Cr ions. This would have the effect of depleting the lattice of oxygen ions and altering the balance of the $Th:O_2$ ratio such that the solubility of Th would increase. The effect of Cr on the diffusion of Th through Ni is less well understood and consequently the diffusion coefficient and solubility of the Th in various Ni-Cr alloys was studied.

CHAPTER 2

THE GROWTH OF THORIA IN NICKEL

2.1 Experimental Determination of Growth Rates

The method used to determine the growth rates of the ThO_2 particles was to heat small samples of T.D. Nickel in a furnace for fixed lengths of time under controlled oxygen partial pressures at 1350°C. The samples were then prepared for study by transmission electron microscopy using an electrolytic thinning technique. Fig. 1 is a schematic representation of the system used for heat treatment. The furnace was heated by six 'Crystalon' hot rods, and due to the need for extremely low oxygen partial pressures a double furnace tube system was used to cut down the diffusion of oxygen from the air through the re-crystallised alumina tube into the gas flowing over the samples (see Fig. 2 for details). The higher oxygen partial pressures were fixed by means of H_2/H_2O ratio that was established by mixing oxygen free nitrogen that has been passed through a water saturator at room temperature, with dried pure hydrogen or a N_2/H_2 mixture. The ratio of N_2/H_2 to N_2/H_2O was controlled by means of two pre-calibrated flow meters, and this gave oxygen partial pressures in

FIG. 1 SCHEMATIC DIAGRAM OF APPARATUS

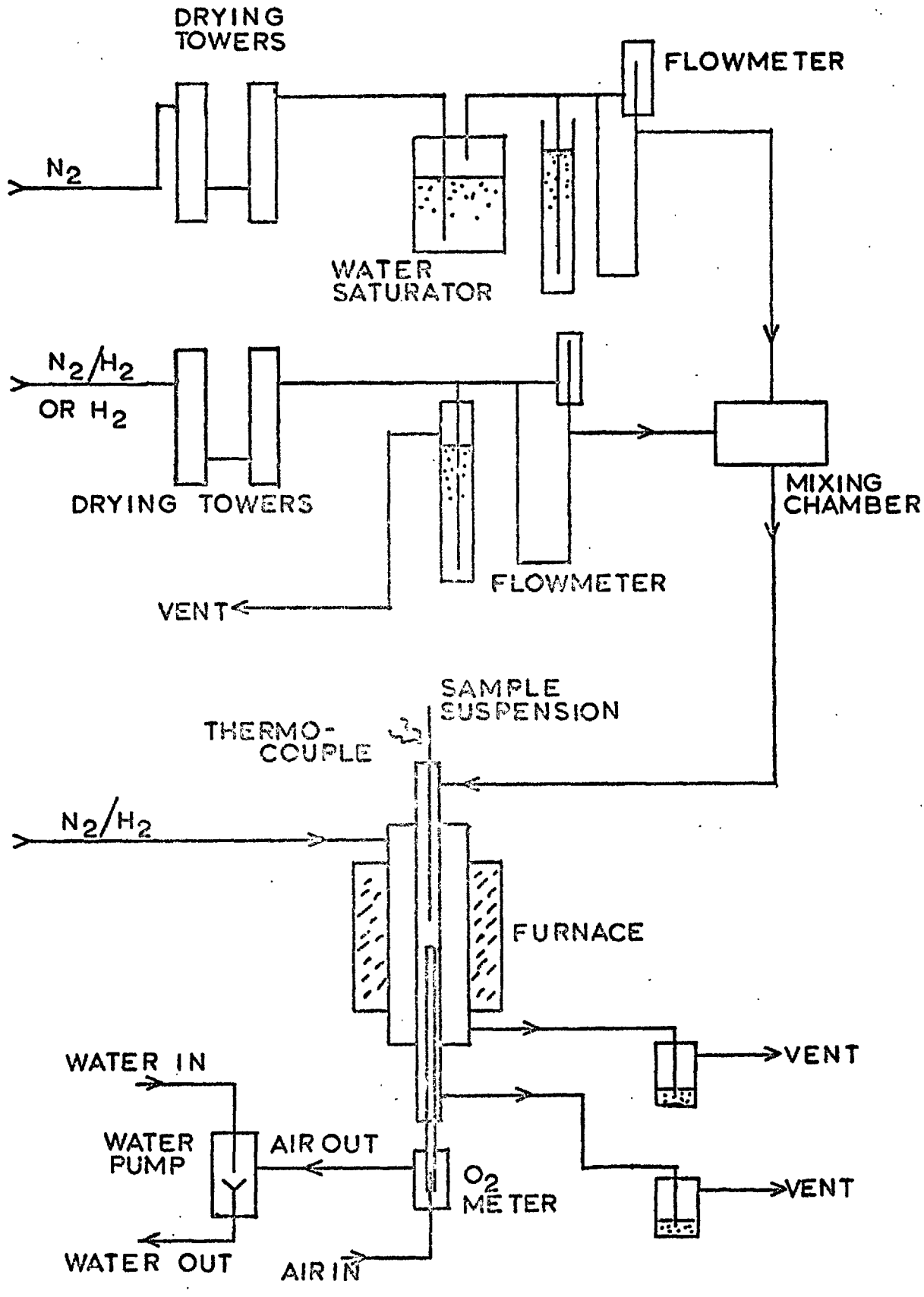

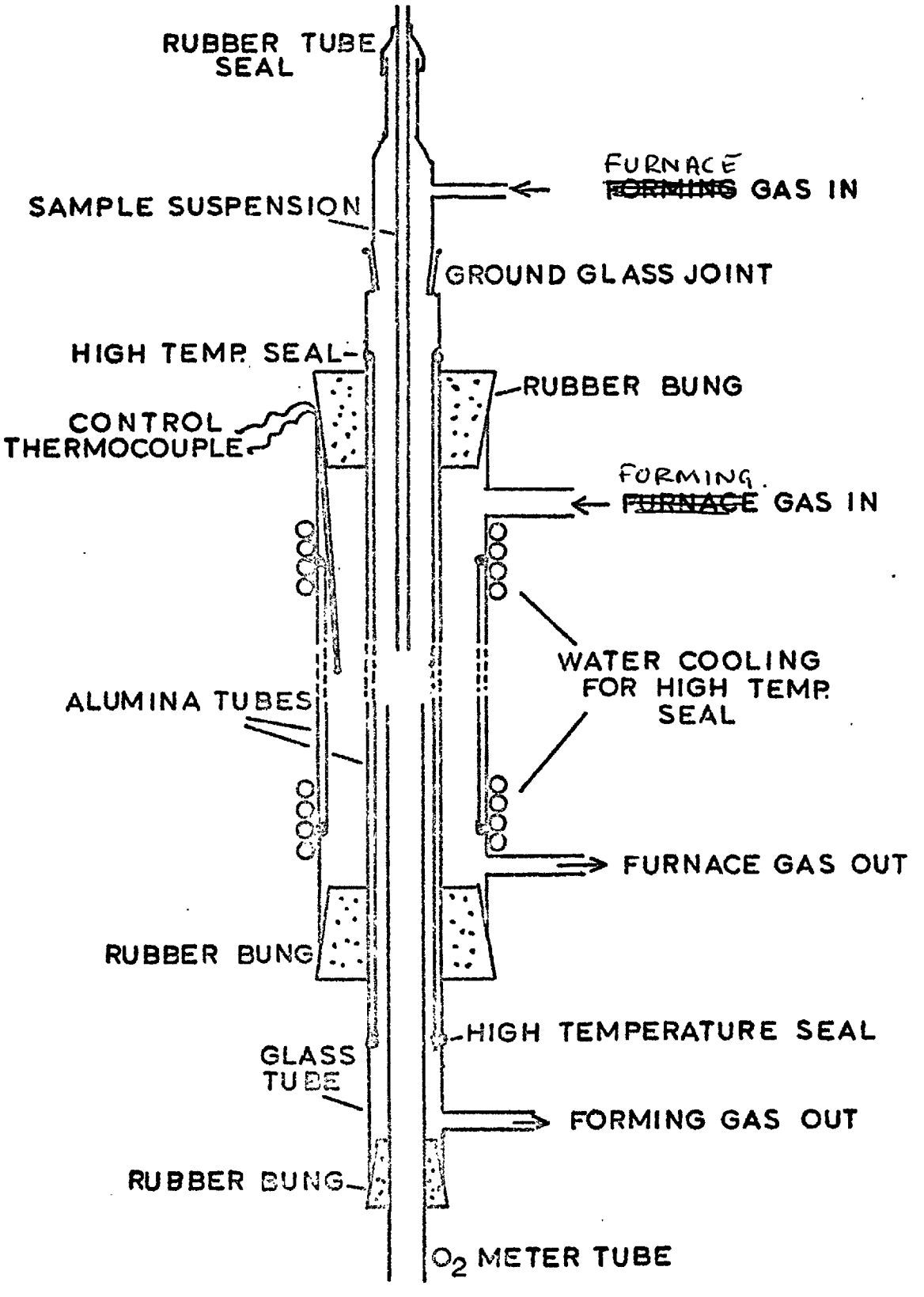

FIG: 2 FURNACE TUBES ARRANGEMENT

the range of 10^{-6}atm. to 10^{-12}atm. which covers the range from the equilibrium PO_2 over a Ni/NiO mixture at 1350°C. to the value that can be reached without forming gas flowing in the outer tube. For very low oxygen partial pressures only the pure dry hydrogen was passed over the sample, and forming gas passed through the outer tube, this gave a lowest value of 10^{-18}atm. which is sufficient to inhibit the formation of Cr_2O_3 on Ni/Cr samples.

2.2 Measurement of Oxygen Partial Pressures

The oxygen potentials of the treatment gas were measured by a solid state electrolyte technique using a ZrO_2/CaO closed end tube. The experimental arrangement is shown in Fig. 3. The electrodes on either side of the cell were (1) a platinum wire wrapped round the outer end of the tube. Contact between the tube and the platinum wire was extremely good because the surface of the electrolyte tube was coated with a thin layer of Ni from the samples which caused the Pt. to wet the surface and give an ideal contact. (2) The inner electrode was the Pt. side of a Pt/Pt 13% Rh thermocouple held into the inner face of the electrolyte tube by a spring loaded Al_2O_3 tube which also carried the reference

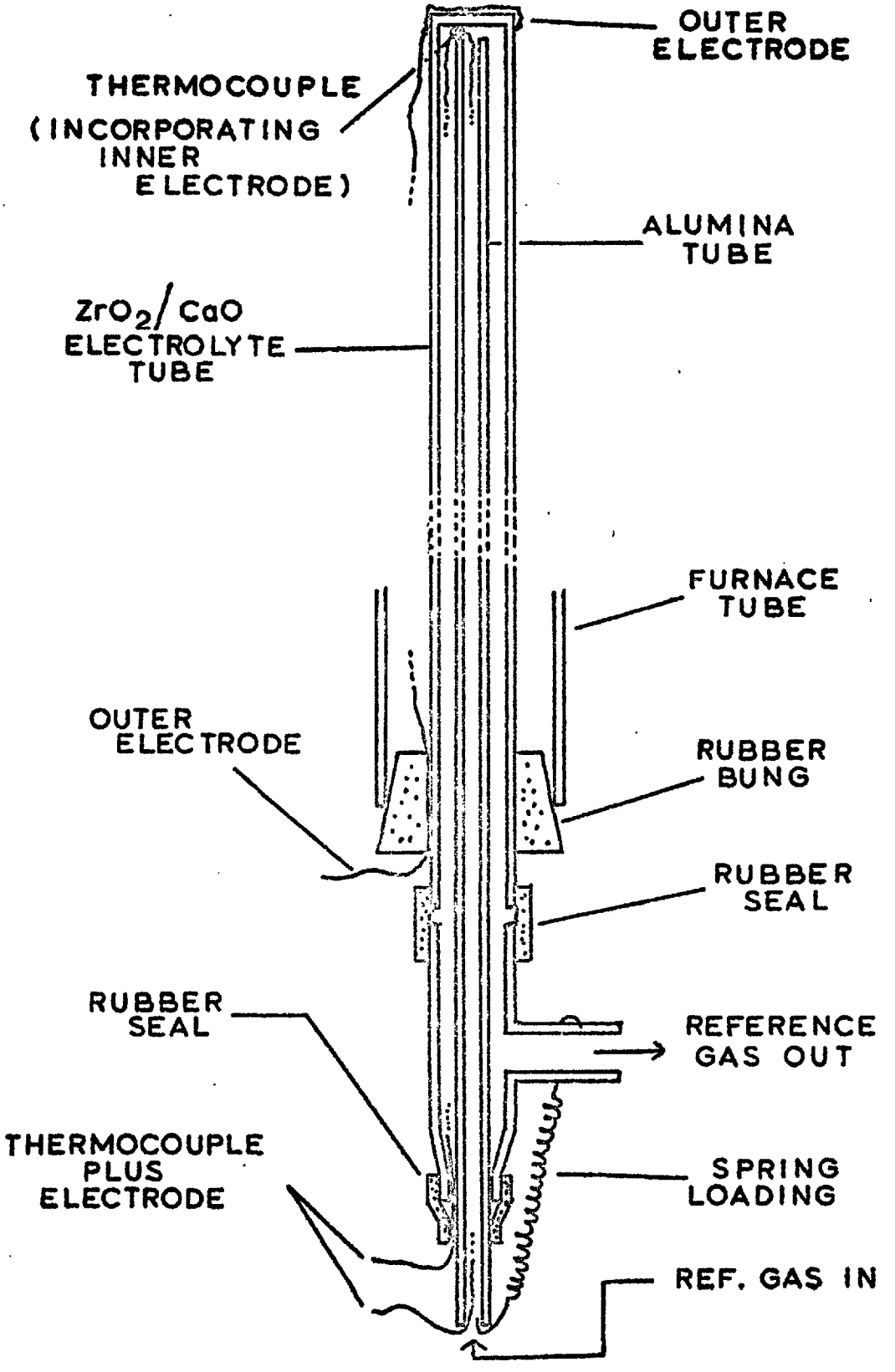

FIG. 3 OXYGEN METER ASSEMBLY

gas there. This thermocouple could then measure the temperature of the cell accurately and also provide one of the electrodes. Air was used as the reference gas because it could easily be supplied to the cell by drawing air through the cell by means of a water pump. The cell then is Furnace gas

Hence, as the E.M.F. across the cell equals:-

$$\frac{R\,T}{4\,F}\,\mathrm{Ln}\,\frac{PO_2 \text{ in the system}}{PO_2 \text{ in the standard gas}}$$

The oxygen partial pressure of the furnace gas can be accurately measured. The output from the cell was determined using a Solatron Type 1M1620 digital volt meter. The values calculated from the gas ratio always agreed with the measured E.M.F. and since room temperature (and consequently the percentage of H_2O in the carrier gas) remained nearly constant a fixed PO_2 could be established. In practice fluctuations in the E.M.F. were typically a little as ∓ 5 mv. in 600 mv. over periods of up to 200 hours.

2.3 Sample Suspension

This is detailed in Fig. 4. The clamping arrangement facilitates the quick removal of the samples during diffusion anneals (see section 4.3), it also enables the

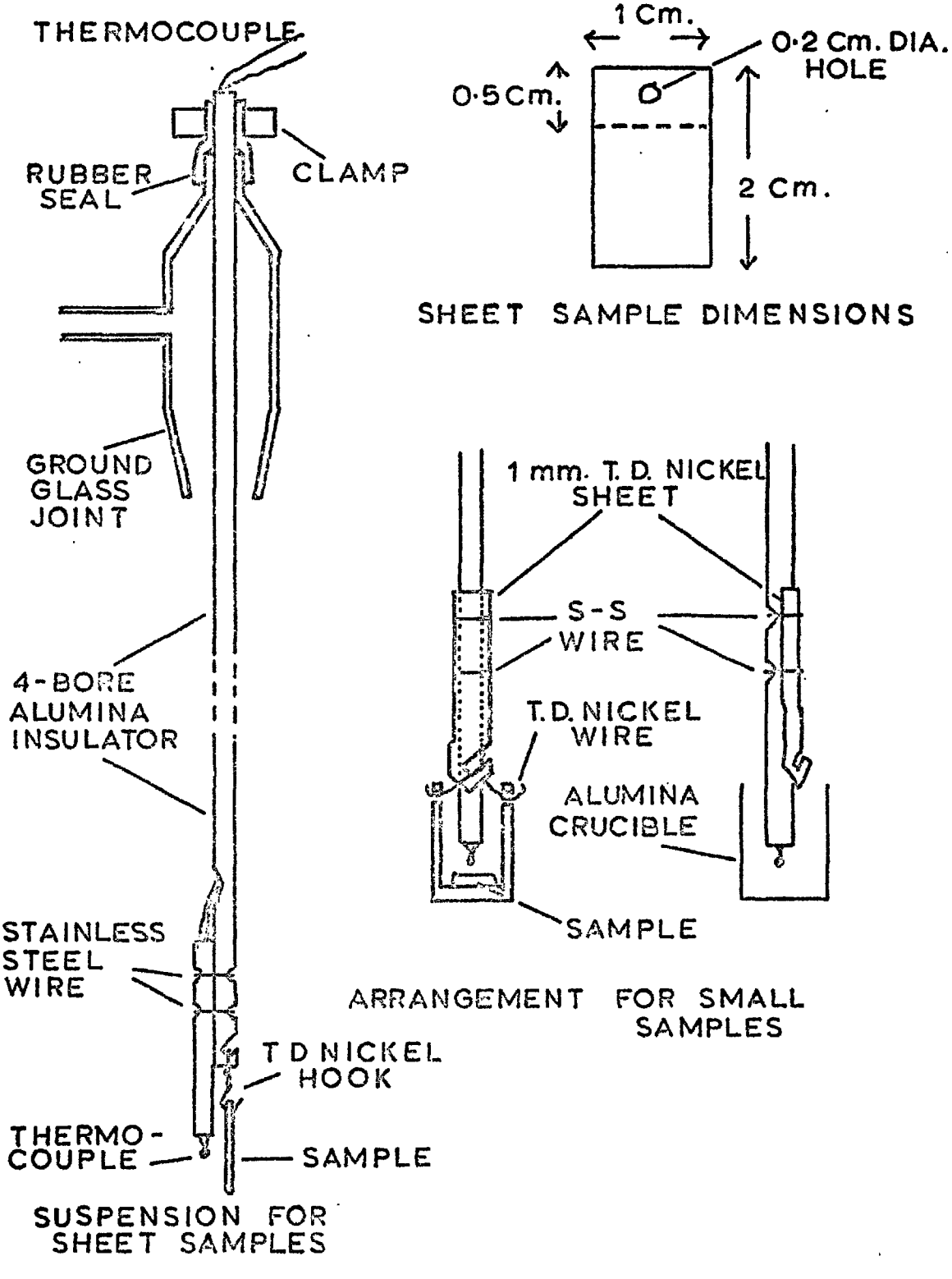

FIG. 4 DETAILS OF SAMPLE SUSPENSION

furnace to be run continuously at temperature to prolong element life.

The samples of T. D. Nickel were typically 1 cm. x 2 cm. x 0·1 cm. (see Fig. 4.) and the thermocouple was always within 0·5 cm. of the sample so the temperature measured was taken as the true sample temperature.

In the case of samples which were suspended in Al_2O_3 crucibles no interaction between the Ni and the Al_2O_3 was noticed. In the case of samples suspended from stainless steel wire the upper section of the sample was discarded to reduce the risk of any possible contaminated material being used.

2.4 Preparation of Samples for Electron Microscopy

On removal from the furnace, samples were ground down from their original thickness of 0·1 cm. to a thickness of 0·02 cm. on SiC paper. This facilitates easier thinning and ensures that any surface contamination is removed. The samples were then thinned electrolytically. In view of the physical dimensions of the samples it was decided to thin the samples by the 'window technique'.

The edges of the sample were then painted with a cellulose - acetate lacquer to stop preferential thinning

at the edges, and then placed in a special holder as shown in Fig. 5. The two anodes were shaped to give preferential thinning at the centre of the sample in order to avoid rupture at the lacquer - metal interface. In order to overcome the increased thinning at the top of the sample, it was turned corner to corner at regular intervals .

The electrolyte used was that recommended by M.v.Heimendahl and G. Thomas [21] namely:-

25% - H_2O

40% - H_3PO_4

35% - H_2SO_4

A series of experiments were carried out to find the best conditions for thinning. This entailed varying the temperature and applied voltage until optimum conditions were achieved.

These were:-

Temperature range	$-5^{\circ}C$	to	$+2^{\circ}C$
Voltage	4V	to	5V
Current density	.25	to	.4 A/Cm^2

These conditions gave a reasonable thinning speed without etching. In view of the heat liberated during thinning (approximately 5 W.) the electrolyte had to be

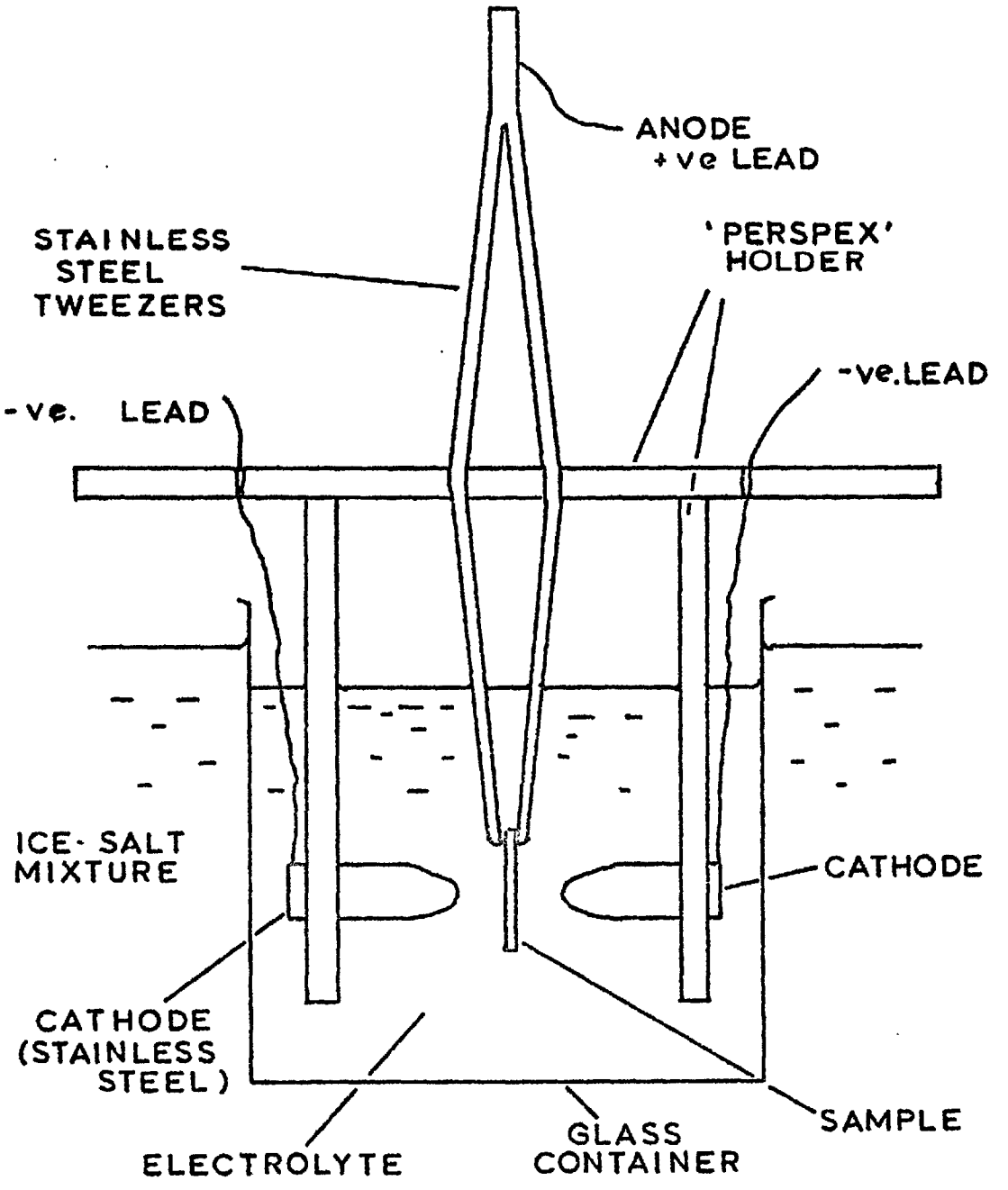

FIG. 5 SAMPLE HOLDER FOR ELECTRO-THINNING.

kept in an ice-salt bath to maintain the temperature at the values quoted above. After a small hole had appeared in the sample sections were cut from around the point of rupture with a scalpel and mounted in grids for study under a Siemens Elmiskop Mk. 1 Electron Microscope. Samples from near the edges of the point of rupture gave good transmission of electrons at 100 KeV and plates were taken of the image at a magnification of 40,000 times.

2.5 Measurement of Particle Size and Calculation of Growth Rate

The 40,000 times magnification of the microscope gave approximately 50 particles per photographic plate so usually three or four plates were taken of different areas (see photographs 1-4). Prints were taken from the plates at an enlargement of 5 times giving a scale of 1 cm. on the print equivalent to 500 Å. The prints were then marked off into areas which contained approximately 10 particles and the diameters of these measured using a calibrated rule. Where particles were non-spherical (Usually less than 10% of the total number) the mean width was taken. In some cases poor thinning restricted the area that could be viewed and consequently the total

number of particles measured was smaller. A histogram of particle sizes was then constructed in order to check that the distribution of radii was consistent with freedom from human measuring bias and the arithmetic mean of the radii found and the results tabulated. A graph of mean radius cubed was plotted against treatment time and the resulting line shows (within the limits of error of measurement) the linear relationship expected.

In order to test the validity of Wagner's equation to growth of the dispersoid it was necessary to know the values of the diffusion coefficient and solubility at a plane interface of Th in Ni. These figures were obtained experimentally as described in a later section.

CHAPTER 3

RESULTS OF GROWTH RATE EXPERIMENTS

3.1 Measurement of Growth Rates

Calculations based on Brown's work show that owing to the large activation energy of Th diffusion, the higher the temperature the greater the growth [27].

Initial experiments at 1200°C. and 1350°C ($PO_2 = 10^{-8}$) showed that after 100 hours there was no measurable increase in the sample heated to 1200°C., whereas the change in mean particle diameter of the sample heated to 1350°C. was statistically significant and agreed with the expected growth. Hence it was decided to carry out all growth rate determinations at 1350°C. which is the highest temperature that can be used when creep and the strength of the sample is considered.

As was outlined in section 1.5 control of the furnace gas oxygen partial pressure is most important in order to give meaningful results and consequently growth rates were measured at four fixed oxygen partial pressures. There were $PO_2 = 10^{-18}$atm., 10^{-14}atm., 10^{-8}atm., and an atmosphere sufficient to oxidise the Ni. Control of the PO_2 over the oxidised Ni is not

critical since as soon as an oxide layer is formed; the oxygen content of the lattice remains constant because of the equilibrium at the oxide-metal interface. The choice of a lower limit of the PO_2 of 10^{-18}atm. was restricted by the apparatus used (see section 2.1).

Samples of T. D. Nickel obtained from Electronic Space Products Inc. were treated as outlined in section 2.2 for times up to 400 hours. The longest treatment time for each PO_2 was calculated as that time which would approximately double the value of $\bar{r}^3$. In view of the long treatment times involved it was thought that any growth during the heating up of the sample would be negligable. The effect due to lattice defects, caused by rolling during manufacture, of possible enhanced particle growth, before being annealed out, is one that could be significant. However, this effect was masked by experimental error and the significance of any such effect was considered minimal.

As can be seen from the Lifshitz-Wagner equation (see section 1.3.) If the growth rates (i.e. $\frac{\bar{r}^3 - \bar{r}_o^3}{t}$) are measured and D and Co evaluated (see section 4.2) a value of γ can be calculated. By comparison of this

value with the values of δ measured by other workers for the ThO_2 (solid) - Ni (liquid) system an estimate of the applicability Lifshitz-Wagner equation to this system can be made.

The results obtained for the variation of $\bar{r}^3$ with time under various oxygen partial pressures are summarised on the next pages. Also included in this results section are four photographs showing typical dispersions of thoria particles in a nickel matrix. Three histograms are included to show the general distribution of particle sizes, data for all the other samples appears in the appendix.

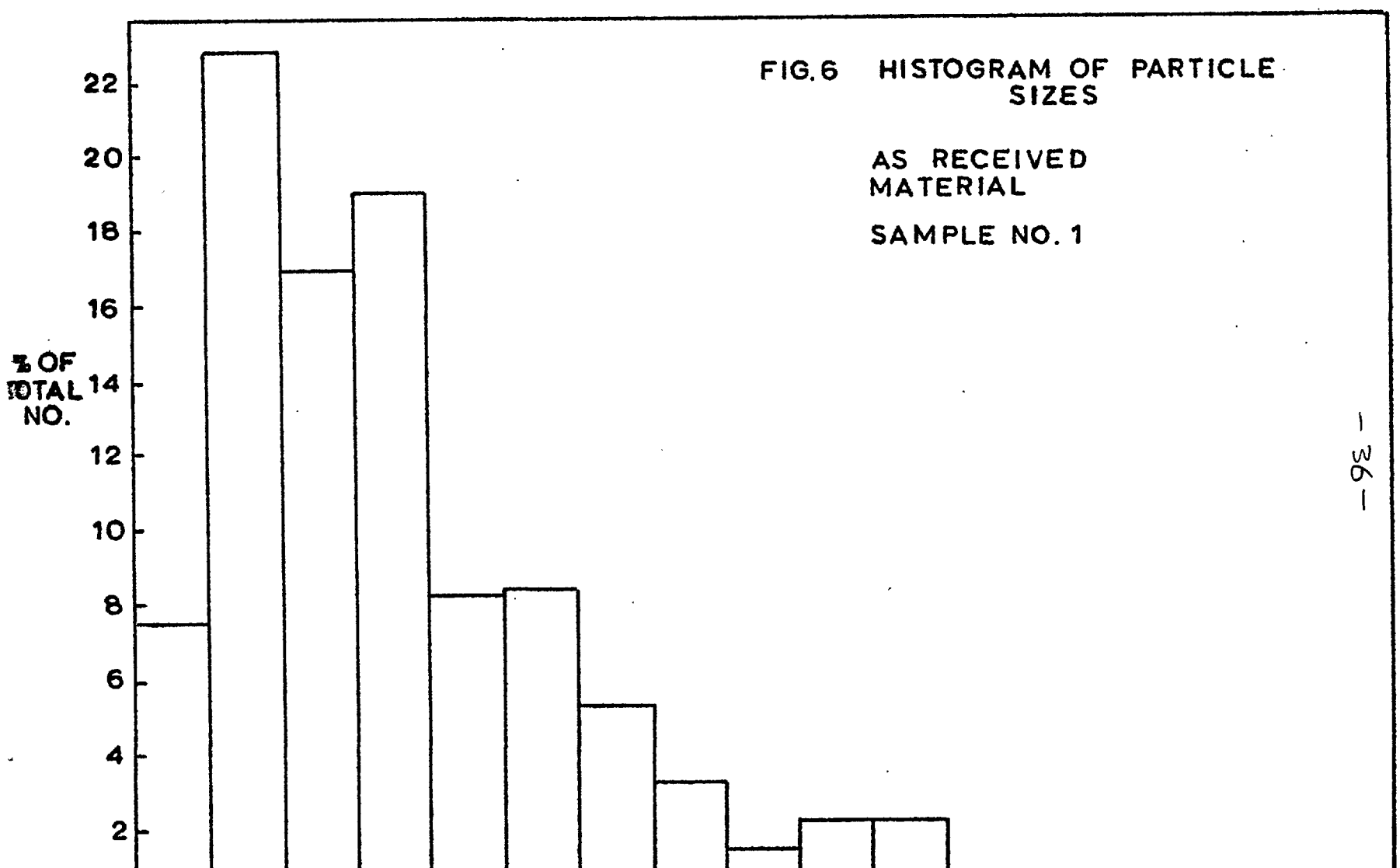
FIG. 6 HISTOGRAM OF PARTICLE SIZES
AS RECEIVED MATERIAL
SAMPLE NO. 1
% OF TOTAL NO.
22
20
18
16
14
12
10
8
6
4
2
0
200
400
600
800
1000
1200
1400
1600
PARTICLE DIAMETER IN Å

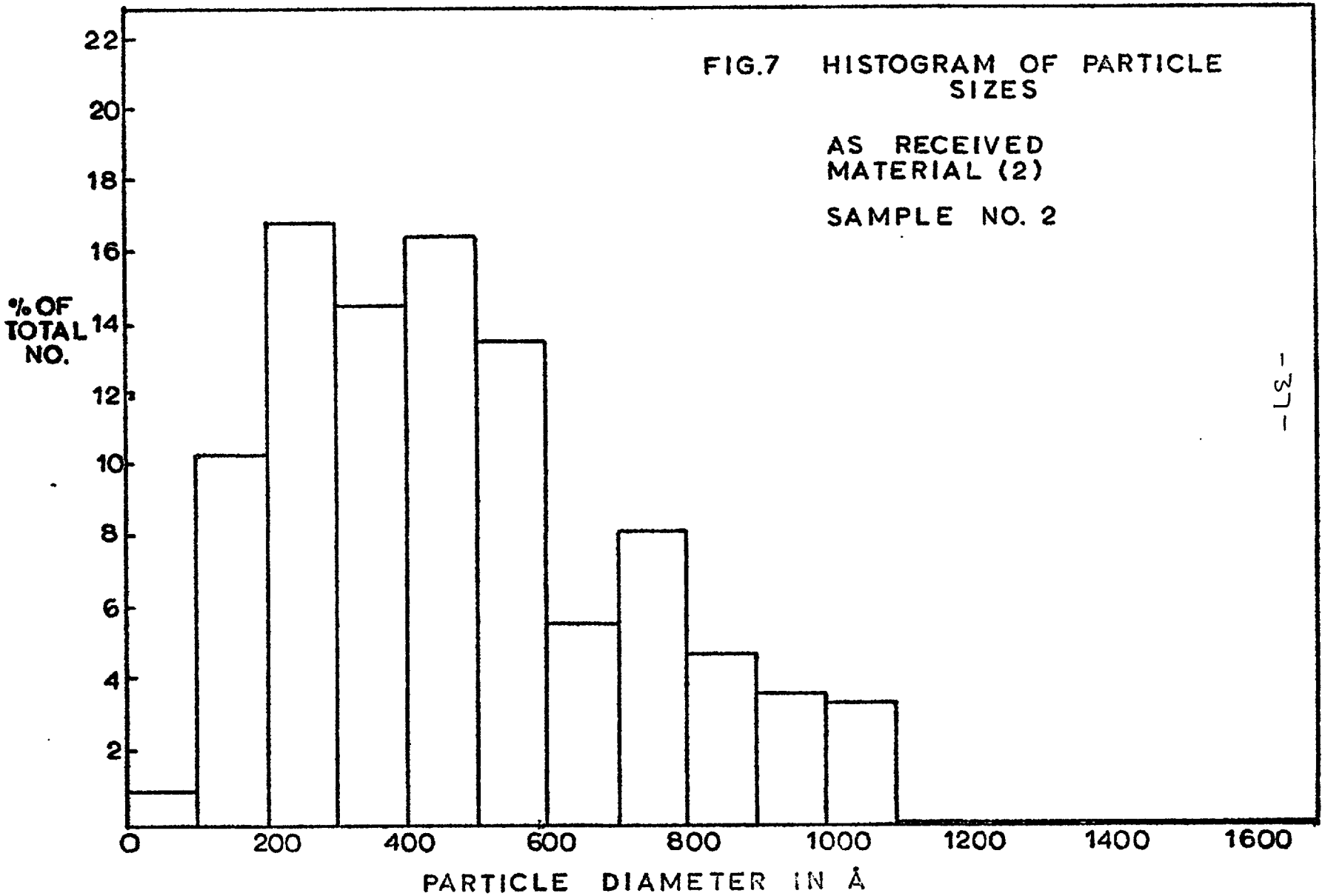
FIG.7 HISTOGRAM OF PARTICLE SIZES
AS RECEIVED MATERIAL (2)
SAMPLE NO. 2
% OF TOTAL NO.
22
20
18
16
14
12
10
8
6
4
2
0
200
400
600
800
1000
1200
1400
1600
PARTICLE DIAMETER IN Å

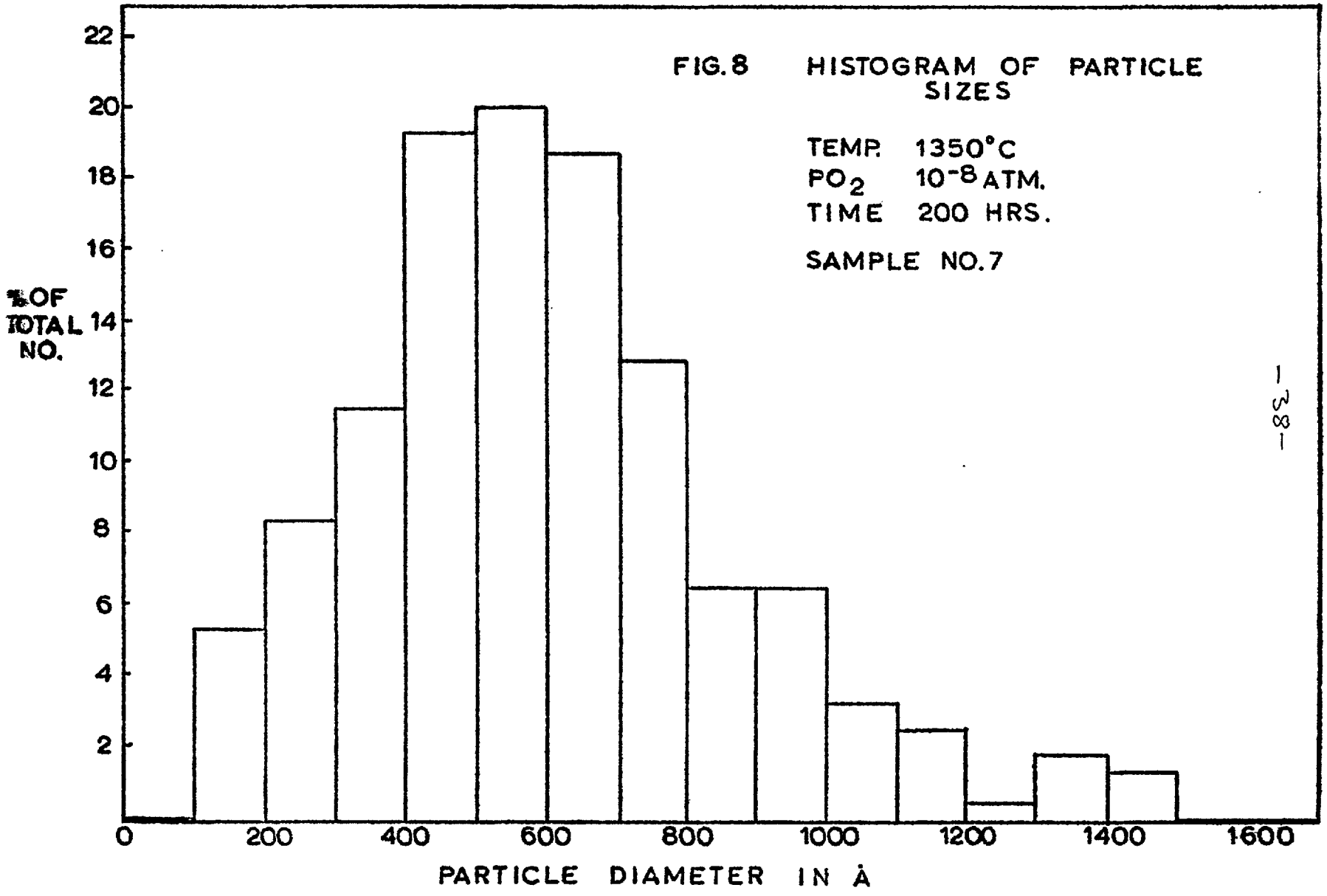
FIG. 8 HISTOGRAM OF PARTICLE SIZES
TEMP. 1350°C
PO_2 10^{-8} ATM.
TIME 200 HRS.
SAMPLE NO. 7
% OF TOTAL NO.
22
20
18
16
14
12
10
8
6
4
2
0
200
400
600
800
1000
1200
1400
1600
PARTICLE DIAMETER IN Å

Summary of results for samples with oxide scale.

Sample No.	Treatment Time	$\bar{r}$ (A)	$\bar{r}^3$ x 10^{18} cm^3
2	0	240·2	13·86
3	50	266·0	18·82
4	100	244·5	14·61

Samples that were heated for times in excess of 100 hours had a very thick oxide layer on them and consequently if was found that very little metal remained. It was therefore impossible to electrolytically thin these samples in order to study the particle growth by electron microscopy. In view of the wide range of mean particle radii of the samples that were treated, no graph has been plotted of $\bar{r}^3$ verus time.

The calculation of growth rates is impossible in these conditions as the evaluation of D and Co by a radioactive tracer technique is only valid under conditions where the surface of the metal is un-oxidised.

Summary of results for $PO_2 = 10^{-8}$ atm.

Sample No.	Treatment Time	$\bar{r}$ (A)	$\bar{r}^3$ x 10^{18} cm^3
1	0	176·1	5·46
5	50	226·3	11·58
6	100	246·5	14·98
7	200	282·0	22·43

Slope of $\bar{r}^3$ versus time = $2{\cdot}283 \times 10^{-23}$ $cm^3 sec^{-1}$

(see Fig. 6)

Regression Coefficient = 0·9922

$D_{(Th\text{-}Ni)}$ at 10^{-8} atm. = $10{\cdot}08 \times 10^{-14}$ $cm^2 sec^{-1}$

$Co_{(Th \text{ in } Ni)}$ at 10^{-8} atm. = $5{\cdot}13 \times 10^{-2}$ Wt. %

$$\gamma = \frac{(\bar{r}^3 - \bar{r}_o^3)}{t} \cdot \frac{9 R T}{8 D Co (Vm)^2}$$

$$\gamma = 2{\cdot}283 \times 10^{-23} \cdot \frac{9.8.314 \times 10^7 .1623}{8.10{\cdot}08 \times 10^{-14} .5{\cdot}13 \times 10^{-2} .0{\cdot}2674}$$

$$\gamma = 2030\ (\pm 1100)\ \text{ergs cm}^{-2}$$

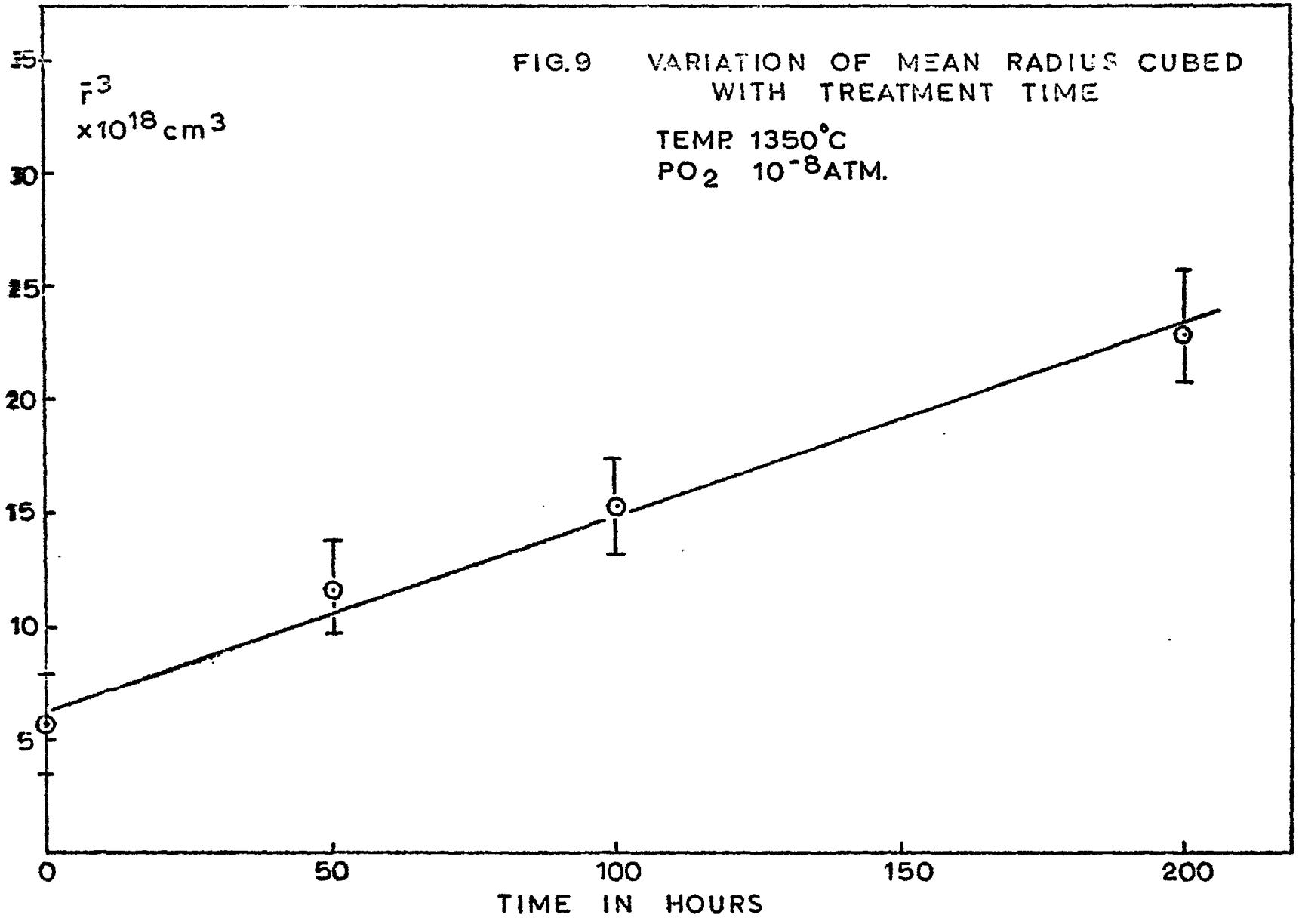
FIG.9 VARIATION OF MEAN RADIUS CUBED WITH TREATMENT TIME
TEMP. 1350°C
PO_2 10^{-8}ATM.
$\bar{r}^3$
$\times 10^{18} cm^3$
35
30
25
20
15
10
5
0
50
100
150
200
TIME IN HOURS

Summary of results for $PO_2 = 10^{-14}$ atm.

Sample No.	Treatment Time	$\bar{r}$ (A)	$\bar{r}^3$ x 10^{-18} cm^3
1	0	176·1	5·46
8	50	198·5	7·82
9	100	205·3	8·65
10	200	230·1	12·28

Slope of $\bar{r}^3$ versus time = $0{\cdot}912 \times 10^{-23}$ $cm^3 sec^{-1}$
(see Fig. 7)

Regression Coefficient = 0·9917

$D_{(Th \text{ in } Ni)}$ at 10^{-14} atm. = $4{\cdot}94 \times 10^{-14}$ $cm^2 sec^{-1}$

$Co_{(Th \text{ in } Ni)}$ at 10^{-14} atm. = $6{\cdot}57 \times 10^{-2}$ Wt. %

$$\gamma = \frac{(\bar{r}^3 - \bar{r}_o^3)}{t} \cdot \frac{9\ R\ T}{8.D.Co\ (Vm)^2}$$

$$\gamma = 0{\cdot}912 \times 10^{-23} \cdot \frac{9.8{\cdot}314 \times 10^7 .1623}{8.4{\cdot}94 \times 10^{-14} .0{\cdot}2674 .6{\cdot}57 \times 10^{-2}}$$

$$\gamma = 1590\ (\mp 880)\ \text{ergs}\ cm^{-2}$$

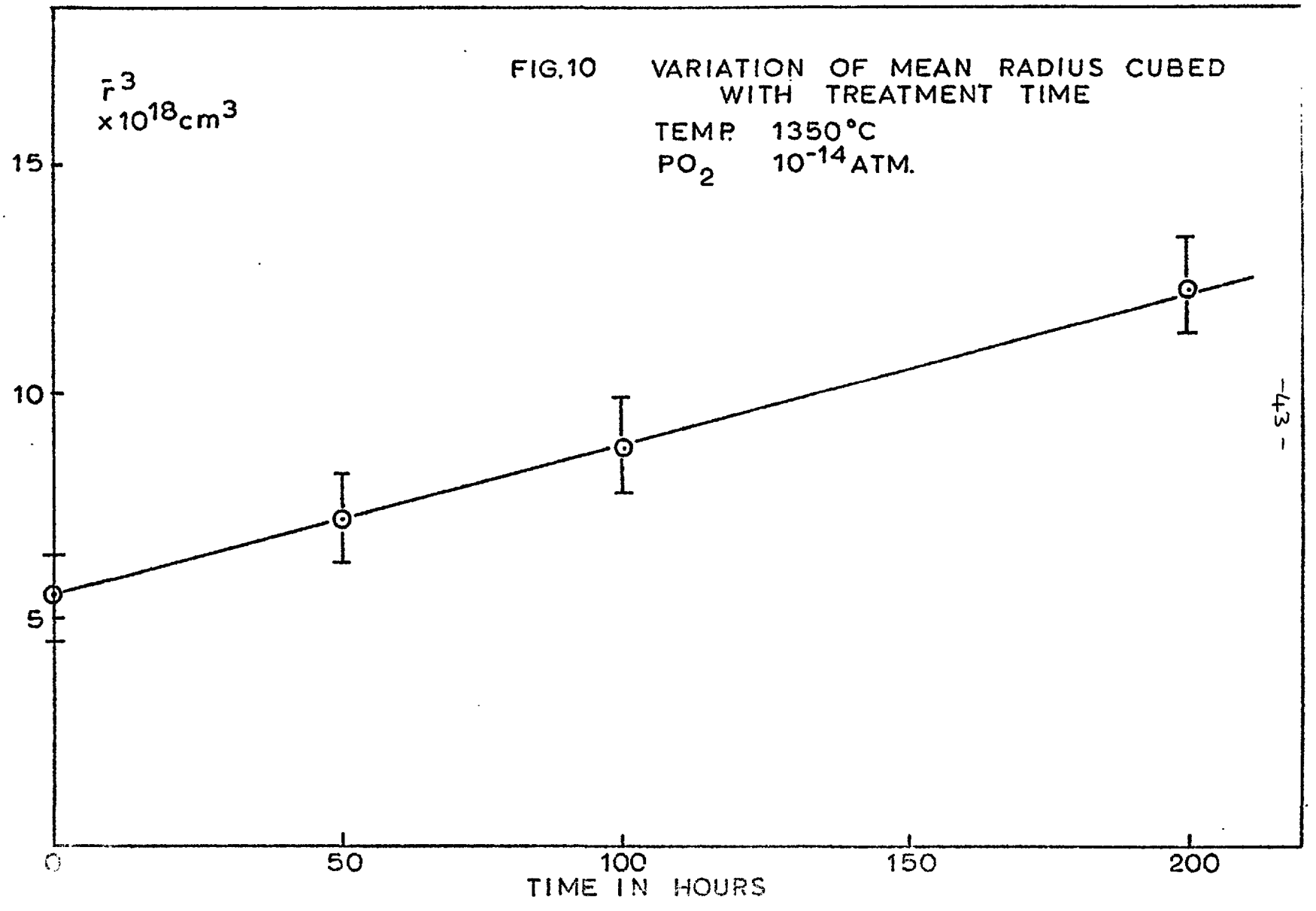

FIG. 10 VARIATION OF MEAN RADIUS CUBED WITH TREATMENT TIME

TEMP. 1350°C

PO_2 10^{-14} ATM.

Summary of results for $PO_2 = 10^{-18}$ atm.

Sample No.	Treatment Time	$\bar{r}$ (A)	$\bar{r}^3$ x 10^{-18} cm^3
2	0	240·2	13·86
11	100	262·9	18·18
12	200	251·5	15·90
13	300	250·2	15·67
14	400	299·6	26·90

Slope of $\bar{r}^3$ versus time = $0{\cdot}654 \times 10^{-23}$ $cm^3 sec^{-1}$
(see Fig. 8)

Regression Coefficient = 0·7233

$D_{(Th \text{ in } Ni)}$ at 10^{-18} atm = $2{\cdot}01 \times 10^{-14} cm^2 sec^{-1}$

$Co_{(Th \text{ in } Ni)}$ at 10^{-18} atm = $4{\cdot}10 \times 10^{-2}$ Wt. %

$$\gamma = (\bar{r}^3 - \bar{r}_o^3) \cdot \frac{9\ R\ T}{8.D.Co\ (Vm)^2}$$

$$\gamma = 0{\cdot}654 \times 10^{-23} \cdot \frac{9.8{\cdot}314 \times 10^7 .1623}{8.2{\cdot}01 \times 10^{-14} .4{\cdot}10 \times 10^{-2} .0{\cdot}2674}$$

$$\gamma = 4505 \text{ ergs } cm^{-2}$$

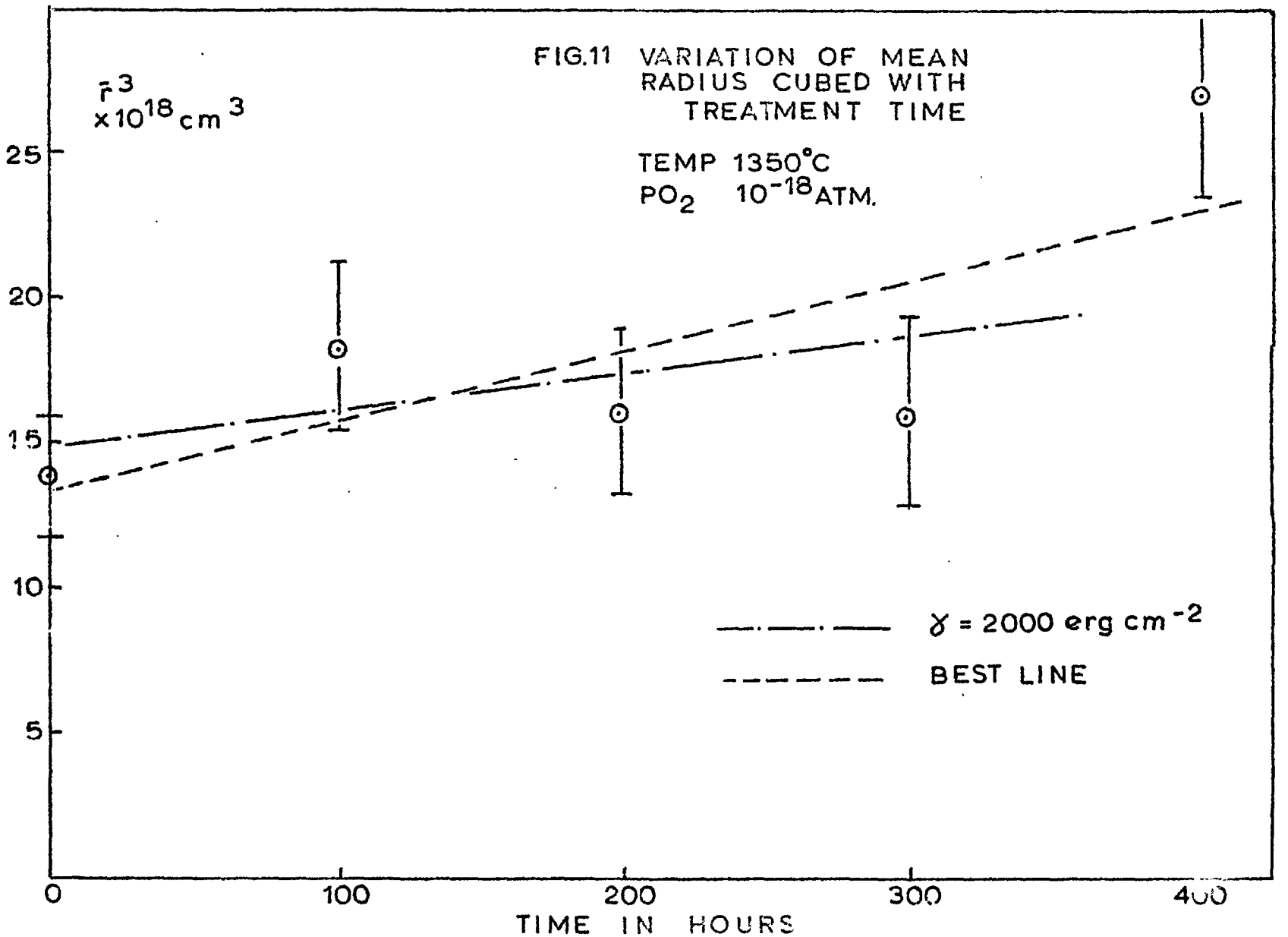
FIG.11 VARIATION OF MEAN RADIUS CUBED WITH TREATMENT TIME
TEMP 1350°C
PO_2 10^{-18}ATM.
$\bar{r}^3$ $\times 10^{18}$ cm^3
25
20
15
10
5
0
100
200
300
400
TIME IN HOURS
γ = 2000 erg cm^{-2}
BEST LINE

As can be seen from the graph of $\bar{r}^3$ versus treatment time for an oxygen partial pressure of 10^{-18}Atm. there exists a wide spread of points. The best straight line found by linear regression analysis (shown as a dashed line) has been used for the calculation of a value for the interfacial energy; also shown on the graph is a line whose slope would give a value for of 2000 ergs cm^{-2}.

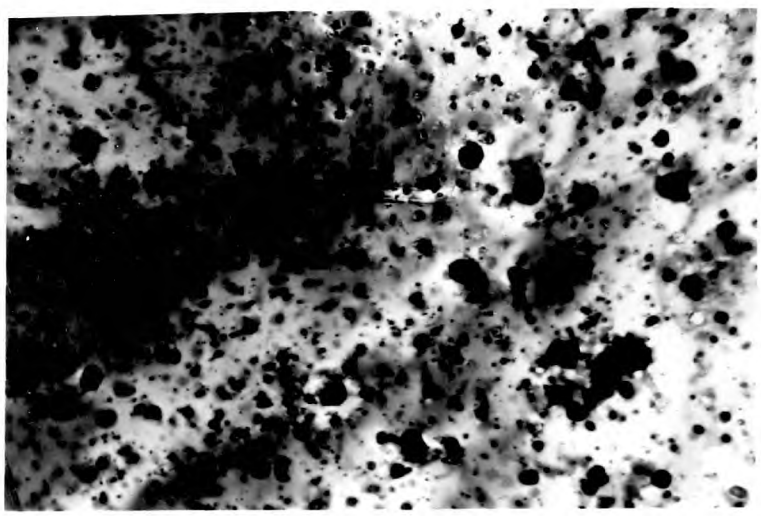

Photograph No. 1

Sample No. 14 400 Hours at $PO_2 = 10^{-18}$ Atm.

Magnification: 1 cm. on photograph represents 1 μm

Photograph No. 2

Sample No. 5 50 Hours at $PO_2 = 10^{-8}$ Atm.

Magnification: 1 cm. on photograph represents 2000Å

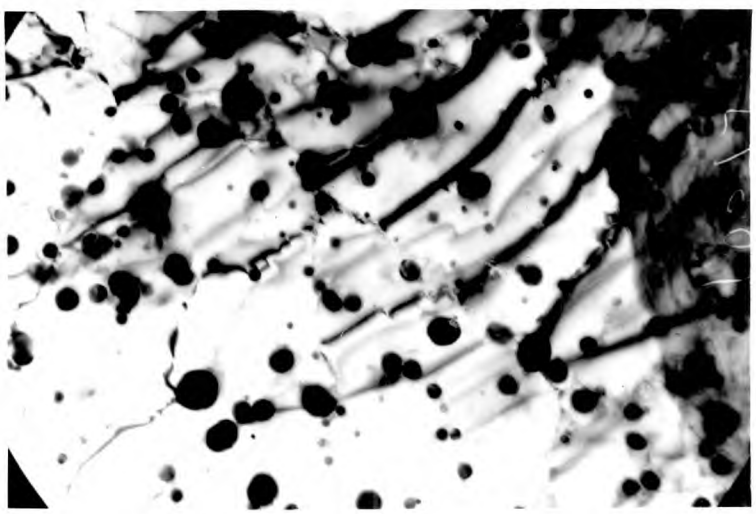

Photograph No. 3

Sample No. 6 100 Hours at $PO_2 = 10^{-8}$ Atm.

Magnification: 1 cm. on photograph represent 2000Å

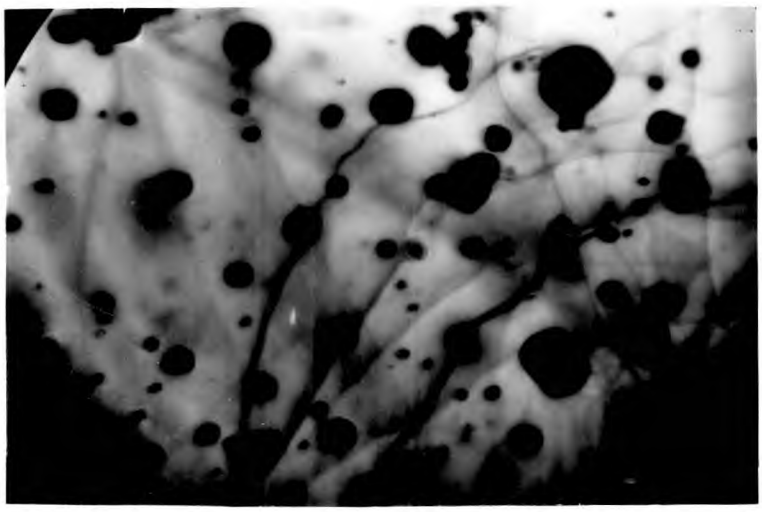

Photograph No. 4

Sample No. 13 300 Hours at $PO_2 = 10^{-18}$ Atm.

Magnification: 1 cm. on photograph represents 2000Å.

CHAPTER 4

DETERMINATION OF SOLUBILITY AND DIFFUSION COEFFICIENTS OF Th IN Ni AND Ni Cr ALLOYS

4.1 Experimental Techniques

Due to the extremely low rate of diffusion of Th in Ni and Ni alloys the only feasible techniques for measuring the diffusion coefficient is one based on a radio-active tracer method. A solution of 12% Th^{230} - 88% Th^{232} was deposited on to sheet samples of Ni alloys as described later, and the samples were then heat treated at 1350°C. for various lengths of time under different fixed oxygen partial pressures, and pure dry hydrogen. After a fixed annealing time the diffusion of the Th was analysed using an alpha-particle spectrometric technique. The spectrometer analysed the energies of the normal radiation from the surface of the sample using a multi-channel pulse height analyser. As the loss in energy from an alpha-particle passing through the Nickel sample is directly proportional to the distance it has travelled in Nickel, the energy spectrum of the alpha-particles gives the relative concentration of Th (i.e. the number of counts) at any diffusion depth (energy loss due to passage through the Nickel from this depth to the surface). This technique

is described in greater details in Section 4.4.

The diffusion equation used to analyse the concentration profiles obtained is that for the diffusion into a infinite cyliner. The diffusion equation is:-

$$C_{(x,t)} = \frac{Co}{2}\left(1 - \text{erf}\ \frac{x}{2\ Dt}\right)$$

Where $C_{(x,t)}$ is the concentration at a depth x from the surface after treatment time t. Co is the equilibrium interface concentration, D is the diffusion coefficient of the diffusing species. This equation is only applicable to a system of two semi-infinite cylinders as long as the concentration change of diffusing species parallel to and adjacent to the interface is negligable.

As can be seen from this equation if a value of Co is assumed a straight line graph of $C_{(x,t)}$ vs. erf $\frac{x}{2\ Dt}$ can be drawn. From the intercept of this graph the true value of $\frac{Co}{2}$ can be obtained and hence the value of D can be calculated for all values of C_x measured. This is discussed in detail in section 5.1.

4.2 Preparation of Samples

Samples of Ni and Ni with five to twenty per cent Cr for these experiments were cut from 0·1 cm. thick sheet

supplied by Henry Wiggin & Co. The samples were the same dimensions as those for the growth rate determinations as the same sample suspension arrangement was used. Samples were cleaned with acetone and dried, and then put into the furnace and annealed for approximately 20 hours at 1350°C. under dry hydrogen for two reasons. The first reason being that the samples had been rolled to their final thickness (20% reduction) and had not been annealed, consequently, there existed a large amount of work-hardening, and thus dislocations, in the material. These dislocations would be removed by heat treatment and also grain growth would be possible. The grain sizes achieved by annealing were of the order of 0·1 to 0·15 cm. and consequently, the possible effect of any preferential grain boundary or dislocation path diffusion is minimized. The second reason for annealing treatment is to remove any oxide or other contamination from the surface and, because thermal polishing takes place at high temperatures, the surface of the sample should be clean and free from imperfections.

The annealed samples were then plated all over one face with a solution containing the radio-active tracer. The tracer used was 12% Th^{230} with 88% Th^{232}. As the

specific activity of Th^{230} (half life equals 8×10^4 years) is much higher than Th^{232} (half life equals $1{\cdot}4 \times 10^{10}$ years) the number of disintegrations due to the Th^{232} is almost negligable. The tracer was supplied as a 5 mg. solution of Th nitiate in 5 mls. of nitric acid.

An alcoholic solution of the tracer was prepared as follows:-

Excess perchloric acid was added to the nitrate solution and this was evaporated to dryness. The residue was then dissolved in pure dry ethyl alcohol. This solution was kept in a bottle with a ground glass stopper to prevent water absorbtion from the atmosphere.

A quantity of the solution was transferred to the clean surface of an annealed sample using a hypodermic syringe. The quantity put on the surface was such that there would be sufficient Th present at the surface of the sample to be considered a semi-infinite source in terms of the diffusion rates involved. The alcoholic solution was then evaporated and the sample kept in a water-free atmosphere till used.

4.3 Solution Treatment of Samples

Samples were suspended in a furnace at 1350°C. for periods of time ranging from 12 to 50 hours under atmospheres

in the range from PO_2 equals 10^{-18}atm. to $PO_2 = 10^{-8}$atm. for pure Ni and only $PO_2 = 10^{-18}$atm. for Ni-Cr samples. The practical arrangement for heat treatment was the same as for the growth rate experiments (see Fig. 1), the sample suspension was also identical to that for growth rate experiments (see Fig. 4). The oxygen partial pressure was controlled and measured as before (see section 2.2).

Initially, samples were allowed to heat up and cool down at the same rate as the furnace (heating time 0°C to 1350°C = 4 hours, cooling time from 1350°C to 1000°C = 40 minutes), but it was felt that faster heating and quenching would give a more accurate assessment of the solution treatment time and also reduce the time for annealing a number of samples, consequently, the following method was used.

The furnace was run up to 1350°C. with nitrogen flowing through the furnace tube with the sample located at the top of the tube. The furnace gas was then changed to forming gas and this gas flushed through the system for 20 minutes. The furnace gas was then changed to the treatment gas and this flushed for 30 minutes. The clamp around the sample suspension rod was then loosened and the sample lowered into the hot zone of the furnace at a

speed such that the temperature rose at a rate of 300°C. a minute.

At the end of a solution treatment this procedure was reversed except that the sample was removed as quickly as was possible.

4.4 Alpha-Particle Spectrometry

As has been mentioned previously, the energy lost by an alpha-particle in passing through any material is directly proportional to the distance travelled in that material. In essence alpha-particle spectrometry consists of the determination of the number of particles that have a specific energy. The equipment used in this experimental programme was the same as that used by Brown[27] and only a brief description of the experimental equipment is given here since a full description is available in the above mentioned work. Alpha-particles from the samples were analysed using a solid state detector (Elliott type SRD 1). This consisted of a n-type silicon single crystal that had a layer of p-type silicon formed on its surface. Electrical contacts were made by means of a thin evaporated layer of gold on the surfaces. By means of these contacts the p-n junction was biassed using a C. & N. (Elect.) Ltd., Type 178D power unit. At the p-n junction there is a "depleted

zone" which is essentially intrinisic in its electrical properties.

As an alpha-particle passes through this zone it forms a number of electron-hole pairs proportional to the energy of the particle. The electron-hole pairs produce a pulse at the electrodes of the detector, necessarily proportional to the particle energy. These pulses were then amplified using a Type 178D Head Amplifier and then fed into an IDL Type 652 wide-band pre-amplifier, and finally into a multi-channel pulse height analyser Type 1363D.

The sample and detector were both in a chamber evacuated by a rotary pump which maintained a vacuum of normally 10^{-3}cm. Hg. As the geometry of the chamber was the same as that of Brown [27] the same solid angle of detection was assumed.

4.5 Calibration of the Spectrometer

When an alpha-particle of initial energy E passes through any material thickness x, the alpha-particle will lose a certain amount of energy due to elastic collisions with the atoms in the material. Thus, all alpha-particles emerging from the material will have an energy of $E-\Delta E$ after passing through a specific thickness x.

The rate of loss of energy of theparticles can be expressed as $\frac{\Delta E}{\Delta x}$ and this ratio can be deduced from the range of the particles in that material i.e.

$$\frac{\Delta E}{\Delta x} = \frac{-E*}{R.}$$

Where E* is the energy of the particles from a particular disintegration and R is the measured range.

In order to calibrate the alpha-particle spectrometer it is necessary to know the correlation between channel width (i.e. the energy band width) and the thickness of material that would produce that energy loss.

It is known that alpha-particles produced from a Th^{230} disintegration have an energy of 4·68 MeV and the range of these particles in air at 20°C. and 1 atmosphere pressure is 3·20 cms. The range of alpha-particles in any material, (assuming pure elastic recoil and no capture of particles by the material atoms), can be expressed by:-

$$Rx = R \text{ air} \left[\frac{\rho \text{ air}}{\rho \text{ x}} \sqrt{\frac{M \text{ x}}{M \text{ air}}} \right]$$

Where:-

Rx is the range in the material

R air is the range in air at S.T.P.

ρ air is the density of air at S.T.P.

ρx is the density of the material

M air is the molecular weight of air

M x is the molecular weight of the material.

The values being:-

ρ air = $1{\cdot}21 \times 10^{-3}$ gm cm^{-3}

ρ Ni = $8{\cdot}8$ gm cm^{-3}

M air = $14{\cdot}4$

M Ni = $58{\cdot}7$

If we substitute these values into the above equation we see that the range of an alpha-particle of energy $4{\cdot}68$ MeV in Nickel is $8{\cdot}60$ microns. Samples of Th^{230} + Th^{232} and U^{233} were then put into the counting chamber and the channel number corresponding to their characteristic energy was noted. Since the radiation from the above materials have specific energies i.e.

Th^{230} - $4{\cdot}68$ MeV

Th^{232} - $4{\cdot}01$ MeV

U^{233} - $4{\cdot}816$ MeV

U^{233} - $4{\cdot}773$ MeV

the width of the channels could be calculated. This gave a value of 66 KeV per channel. Using the fact that a loss of $4{\cdot}68$ MeV is equivalent to a depth of $8{\cdot}60$ microns, the thickness of material equivalent to the energy loss

represented by one channel was calculated. Unfortunately, this equipment did not give an equal number of counts in each channel when a homogenous source was used. The fall off in number of counts over the first 25 channels amounted to 25% of the surface count in a linear fashion so the thickness of material equivalent to each channel had to be altered to compensate for this effect.(See table 1 in the Appendix for corrected channel thicknesses).

Owing to the geometry of the counting chamber and the sample size, the collimation of the alpha-particles was not perfect and consequently not all the particles that were counted had left the surface normally. However, a calculation of the possible error showed that this effect would have had a maximum effect of increasing the count by 0·5% so, as this error was well within other experimental errors in the determination of D, its effect was ignored.

4.6 Instrumental Error in Channel Resolution

When a mono-energetic sample of Th^{230} was placed in the detector chamber the resultant display on the multi-channel pulse height analyser showed that, although all the particles should have been sorted into a single energy channel, there was an appreciable spread of counted particles that apparently had lower or higher energies

than the expected value. Some of the lower energy particles could be expected in view of the fact that the plated layer of the mono-energectic tracer was of finite thickness and hence some of the alpha-particles had lost some of their energy in passing through the plated layer. However, the presence of particles with apparently higher energies can only be due to an instrument inability to correctly sort all the particles into the same energy band. The actual energy spread obtained (after removal of expected background counts) is seen in table 2 in the appendix. As can be seen the number of particles with higher energies than expected is of the form of a Normal Gaussian curve. The counts of particles with lower energies than expected shows a 'tail' which is thought to be due to energy loss in travelling through the plated layer. In order to use the values obtained to correct the experimental values only the high energy portion of the curve was used for analysis of the errors involved. The actual method of analysis is given in detail in Section 5.1.

As the instrumental error in channel sorting affects the true channel counts it was impossible to accurately analyse the counts in any channel nearer the surface than channel 6 from the peak. Although only the nearest two

channels to the peak are considered for the estimation of actual channel errors, in terms of the actual counts measured, i.e. a peak count of the order of 10^4 counts, the error involved in terms of the actual channel counts, i.e. approximately 500 in channel 6, the effect of the surface tracer layer is non-negligable until a distance greater than that represented by channel 5 from the surface.

4.7 Method of Analysis of Concentration Profiles

When the number of counts in each channel had been obtained after a known counting time it was necessary to subtract from each individual channel the total counts due to the background radiation (usually contamination of the sample holder in the counting chamber.).

The background count was found at periodic intervals throughout the experimental programme by placing an unplated sample in the chamber and the number of particles emitted was counted over a long period of time. (see table 3 in the appendix). The background profile was then subtracted from the counts measured from each sample that had been annealed and a true value of the counts obtained.

Due to the instrumental errors involved in counting (see section 4.6) it would have appeared necessary to

correct the number of counts obtained in each channel. However, the errors involved in the mis-sorting of pulses of the same height, were eliminated as each channel had approximately the same number of pulses mis-sorted into adjacent channels as it received from the two channels on either side. This assumption is based on a linear relationship between channel count and channel number, obviously the relationship obtained would be consistent with the diffusion curve, but the errors involved is assuming linearity were overshadowed by the errors in the spread of channel counts around the curve expected from the diffusion equation and consequently were ignored.

CHAPTER 5

DIFFUSION OF Th IN Ni AND Ni-Cr.

5.1 Analysis of Diffusion Results

The equation used for the interpretation of the results obtained was:-

$$C_{(x,t)} = \frac{Co}{2}\left(1 - \text{erf}\ \frac{x}{2\sqrt{Dt}}\right)$$

As can be seen there are two unknowns, Co and D in this equation, therefore it is necessary to convert the equation to a linear form in order to eliminate one of the variables. The method used for analysis was as follows:-

A value of 10,000 counts was assumed for $Co/_2$ and the value of $\left(1 - \frac{Cx}{10,000}\right)$ evaluated. This figure is equal to $\text{erf}\left(\frac{x}{2\sqrt{Dt}}\right)$ However, the value of an error function can be expressed in terms of the normal curve of error.

The relationship between the two is:-

$$\tfrac{1}{2}\ \text{erf}\left(\frac{t}{\sqrt{2}}\right) = \int_0^t \phi(x)\ dx.$$

Hence from the area under the normal curve the value of $\left(\frac{x}{2\sqrt{Dt}}\right)$ can be evaluated. (Shown as t* in the results).

Consequently, the intercept of a graph of

$$\text{erf}^{-1}\left(1 - \frac{Cx}{10,000}\right) \text{ vs. (channel No.)}$$

would give a true value of $\frac{Co}{2}$ from the intercept at channel number equals 0.

This value of $\frac{Co}{2}$ was then substituted back in the original equation and a value of D calculated for each channel number using the value of t, the treatment time, and x, the equivalent thickness of each channel (see appendix for values).

5.2 Calculation of Interfacial Solubilities

Once the value of $Co/_2$ is computed, the interfacial solubility can be calculated as follows:-

area of sample = (x) cm^2

First channel thickness = 0·123 microns (see table 1 in the appendix)

Therefore

volume of first channel = (x) x 0·123 x $10^{-4} cm^3$

and as the density of Nickel = 8·88 gm. cm^{-3}

Therefore

Weight of Nickel in first channel = 0·23 (x) x 8·88 gms

Solid angle of detection (see Ref. 27) = 0·0519 π

Total counts for first channel $= \frac{4}{0 \cdot 0519}$ Co

The number of disintegrations per second in a radioactive decay is defined by:-

$$C^* = \frac{N \lambda y}{M}$$

Where:-

N is Avagadro's Number

λ is the radioactive decay constant for the material

y is the weight of material

and M is the molecular weight

as $\lambda = \frac{0 \cdot 694}{t^{\frac{1}{2}}}$

Where $t^{\frac{1}{2}}$ is the half life of the active species.

We can write:-

$$C^* = \frac{N.y.\ 0 \cdot 694}{M\ t^{\frac{1}{2}}}$$

Hence, if N, M, C^* and $t^{\frac{1}{2}}$ are known y can be calculated. Combining this equation with the expression for the total count in the first channel we have:-

$$C^* \cdot \frac{4}{0 \cdot 0519} = \frac{N \times 0 \cdot 694 . y}{M . t^{\frac{1}{2}}}$$

M for Th^{230} = 230.

$t^{\frac{1}{2}}$ for Th^{230} = $8 \cdot 0 \times 10^4$ years

Aragadro's Number = $6 \cdot 023 \times 10^{23}$

Hence the weight of the Th^{230} equivalent to the total 4π count is:-

$$= \frac{C^{*}.4.230.80.10^{4}.365.24.60.60.}{0{\cdot}0519.6{\cdot}023.10^{23}.0{\cdot}694}$$

$$= 1{\cdot}07 \times 10^{-7}\ C^{*}$$

As the plating solution was 12% Th^{230}

Hence the total weight of thorium in solution at the interface

$$= \frac{100}{12} \cdot 1{\cdot}07.10^{-7}C^{*}$$

$$= 8{\cdot}93 \times 10^{-7}C^{*}$$

Therefore the interfacial solubility by weight is

$$= \frac{8{\cdot}93.10^{-7}C^{*}}{0{\cdot}123.8{\cdot}88(x).10^{-4}}$$

$$= 8{\cdot}16 \times 10^{-3}\frac{C^{*}}{(x)}$$

$$= 8{\cdot}16\frac{C^{*}}{(x)}.10^{-1}\ \text{Wt. \%}$$

5.3 Results for Thorium Diffusion in Ni with 0%, 5%, 10%, 15%, 20% Cr.

The values obtained are summarised in the following pages. Fig. 12 shows the equilibrium interfacial solubility of thorium (in Wt. %) versus Cr percentage and Fig. 13 shows the calculated diffusion coefficients at 1350°C. versus percentage of chromium in the samples. The tables following these graphs summarise the results and following these tables are the results obtained for Th diffusion in pure Ni at oxygen partial pressures of 10^{-8}atm., 10^{-14}atm. and 10^{-18}atm. which were used in the determination of the growth rates in Chapter 3. A complete tabulation of the experimental results for the determination of the diffusion coefficient and solubility of Th in Ni - Cr alloys is shown in the appendix.

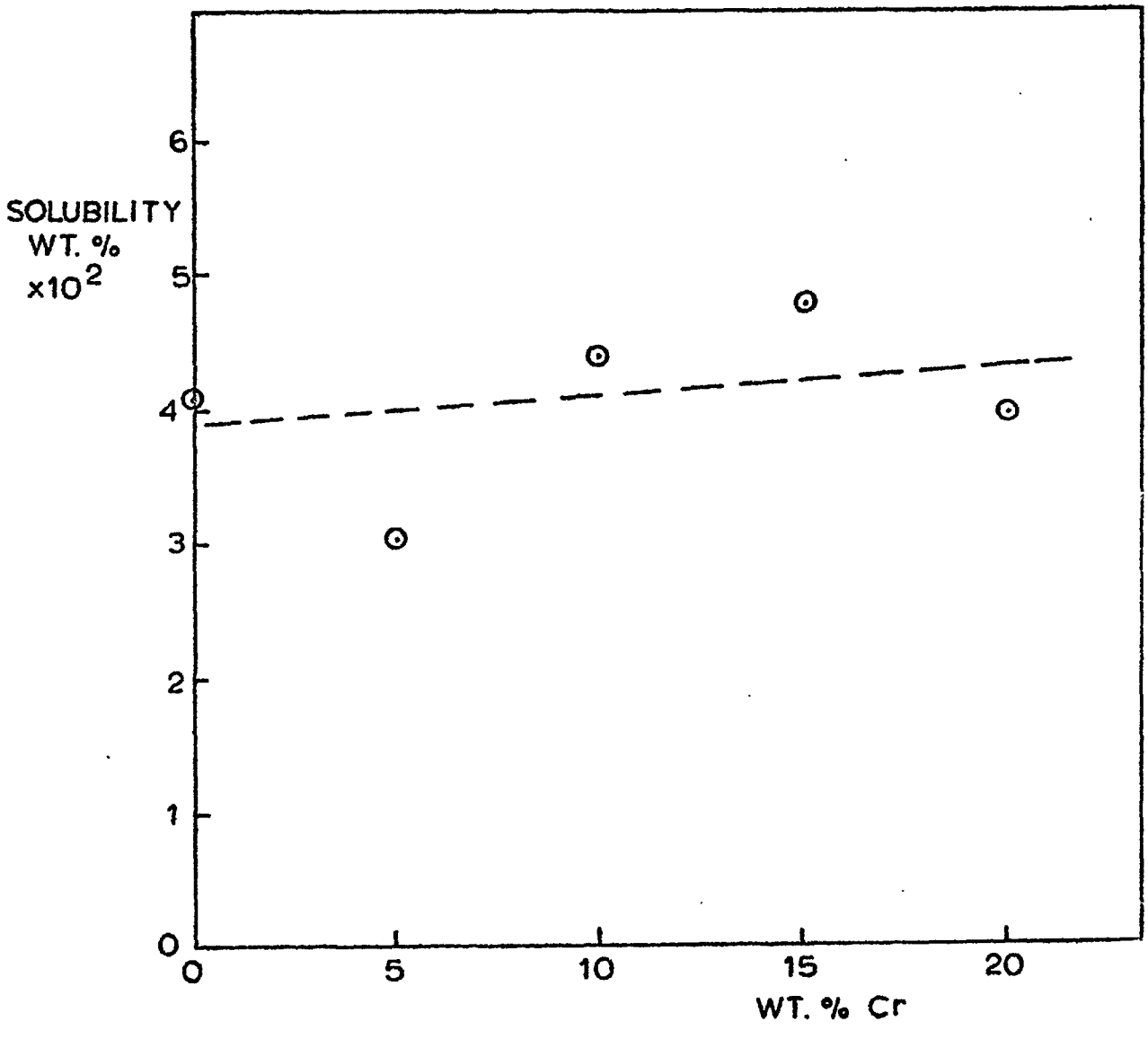

FIG.12 SOLUBILITY OF THORIUM IN Ni-Cr.

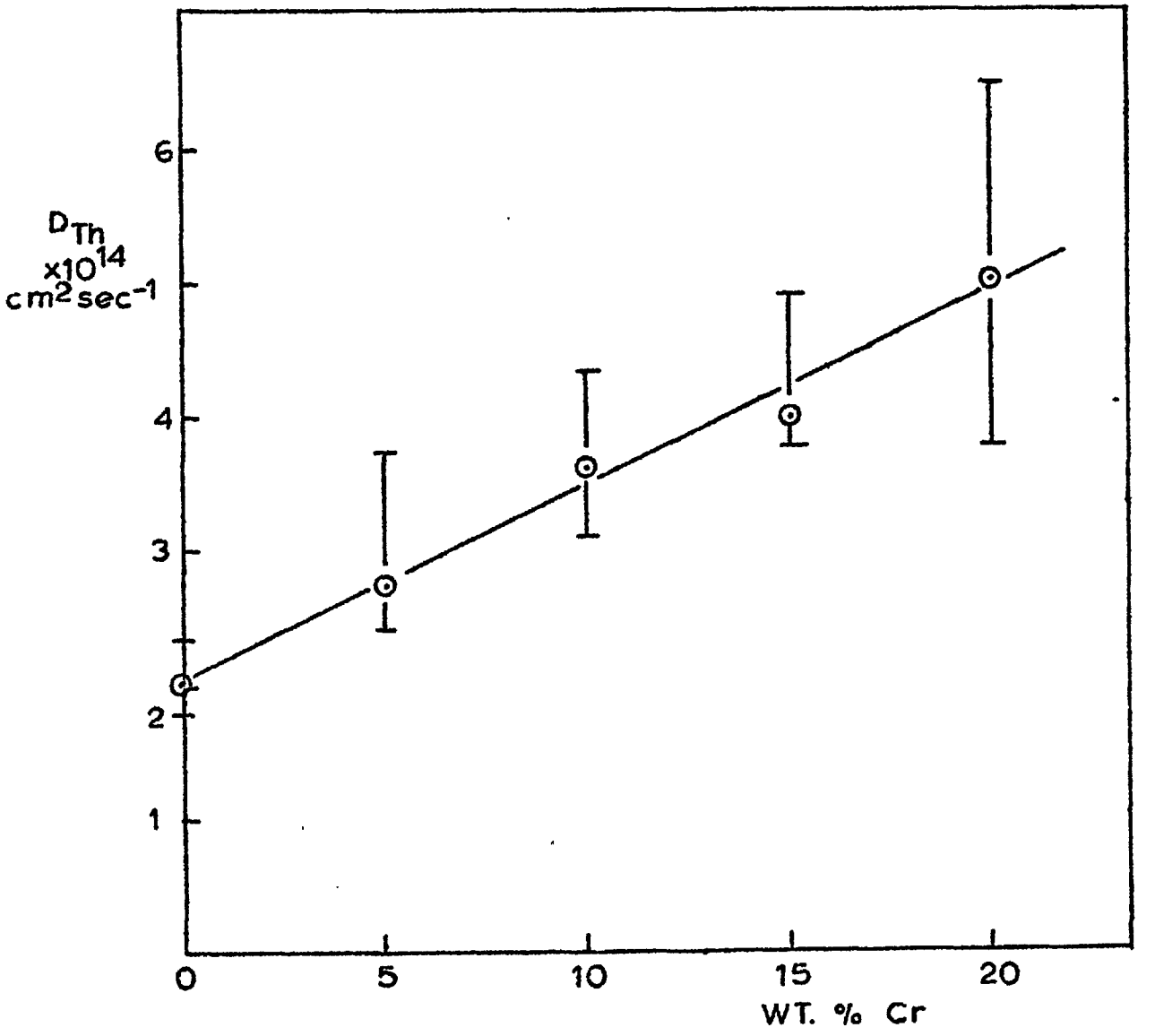

FIG.13 DIFFUSION COEFFICIENT OF THORIUM IN Ni-Cr

Summary of solubility of Th in Ni - Cr alloys at 1350°C. under an oxygen partial pressure of 10^{-18}atm.

Wt. % Cr	Solubility of Th in Wt. % x 10^2
0	4·10 (∓ 0·24)
5	3·06 (∓ 0·10)
10	4·42 (∓ 0·12)
15	4·79 (∓ 0·10)
20	4·00 (∓ 0·12)

(see Fig. 12)

Th diffusion in Ni - Cr

Wt. % Cr	D x 10^{14} $cm^2 sec^{-1}$
0	2·01 (∓ 0·35)
5	2·74 (∓ 1·02)
10	3·62 (∓ 0·73)
15	4·05 (∓ 0·81)
20	5·03 (∓ 1·22)

(see Fig. 13)

SAMPLE NO. 15 Pure Ni

$PO_2 = 10^{-8}$ Atm. Anneal time = $3 \cdot 69 \times 10^4$ sec

Channel No.	Channel Counts	t*	D $\times 10^{14}$ $cm^2 sec^{-1}$
6	1452	1·029	6·33
7	1099	1·131	6·65
8	860	1·213	7·14
9	728	1·268	8·00
10	644	1·308	9·13
11	562	1·351	10·15
12	494	1·390	11·16
13	463	1·411	12·60
14	436	1·427	14·05
15	412	1·445	15·58
		Mean D	10·08

Regression Coefficient = 0·9611

Intercept = 0·8384

$Co/_2$ = 5534 counts

Sample Area = 2·0 cm^2

Counting time = $8 \cdot 826 \times 10^4$ sec

Co* = $6 \cdot 2\ 7 \times 10^{-2}$ counts sec^{-1}

Solubility = $5 \cdot 13 \times 10^{-2}$ Wt. %

Diffusion Coefficient = $10 \cdot 08\ (\pm\ 5 \cdot 5) \times 10^{-14}$ $cm^2 sec^{-1}$

SAMPLE NO. 16 Pure Ni

$PO_2 = 10^{-14}$ Atm. Anneal time = $20{\cdot}16 \times 10^4$ sec.

Channel No,	Channel Counts	t*	D $\times 10^{14}$ $cm^2 sec^{-1}$
6	360	1·775	4·723
7	300	1·821	4·159
8	279	1·842	4·637
9	276	1·846	5·693
10	195	1·930	4·080
11	168	1·959	4·116
12	156	1·973	4·504
13	141	2·001	4·752
14	171	1·959	6·713
15	135	2·015	6·003
		Mean D	4·938

Regression Coefficient = 0·9473

Intercept = 1·6361

$Co/_2$ = 618 counts

Sample Area = 0·285 cm^2

Counting time = $5{\cdot}4 \times 10^4$ sec

Co* = $2{\cdot}28 \times 10^{-2}$ counts sec^{-1}

Solubility = $6{\cdot}57 \times 10^{-2}$ Wt. %

Diffusion Coefficient = $4{\cdot}94\ (\mp 1{\cdot}78) \times 10^{-14}$ $cm^2 sec^{-1}$

SAMPLE NO. 17 Pure Ni

$PO_2 = 10^{-18}$ Atm. Anneal time = $21{\cdot}43 \times 10^4$ sec.

Channel No.	Channel Counts	t*	D $\times 10^{14}$ $cm^2 sec^{-1}$
6	1640	0·986	2·36
7	1150	1·114	1·84
8	879	1·206	1·78
9	666	1·295	1·75
10	536	1·365	1·83
11	444	1·421	1·93
12	315	1·524	1·88
13	293	1·542	2·10
14	276	1·559	2·35
15	201	1·648	2·31
		Mean D	2·01

Regression Coefficient = 0·9832

Intercept = 0·6342

$Co/_2$ = 3698

Sample Area = 2 ·28 cm^2

Counting time = $6{\cdot}45 \times 10^4$ sec

Co* = $11{\cdot}46 \times 10^{-2}$ counts sec^{-1}

Solubility = $4{\cdot}10 \times 10^{-2}$ Wt. %

Diffusion Coefficient = $2{\cdot}01\ (\pm 0{\cdot}35) \times 10^{14}$ $cm^2 sec^{-1}$

CHAPTER 6

MEASUREMENT OF GROWTH RATE PARAMETERS FOR A Ni-Cr-Pt ALLOY

6.1 Introduction

In view of the high affinity of chromium for oxygen and the consequent decrease in free oxygen in the lattice. (see section 1.5) it was thought that the addition of a metal that has a low affinity for oxygen to the alloy would decrease the thorium solubility and consequently decrease the growth rate of ThO_2 particles. Since the addition of noble metals such as gold depresses the melting point of the alloy it was decided to measure the growth rate parameters of a Ni-Cr-Pt alloy.

6.2. Experimental Determination of Diffusion Coefficient and Solubility

The measurement of the diffusion coefficient and solubility of Th in a Ni 80% - Cr 10% - Pt 10% alloy was carried out using the same apparatus and method as described for Ni-Cr alloys in Chapters 4 and 5. In order to prevent oxidation of the surface of the alloy the experiments were carried out under an oxygen partial pressure of 10^{-18} atm. and in order to make comparisons between these results and results for Ni and Ni-Cr the same temperature was used. Samples of a Ni-Cr-Pt alloy

were prepared from Ni-Cr alloy as used in the previous experiments and platinum sheet supplied by Johnson Matthey and Co. Ltd. The alloy was made by melting the constituent metals at 1600°C. under pure dry hydrogen in an alumina crucible using the sample suspension shown in Fig. 4. The melt was held at temperature for two hours in order to ensure complete mixing. The alloy was then cooled over a period of four hours and then sectioned and analysed by electron probe micro-analysis to confirm homogenity. Although this analysis showed slight segregation of Pt to the grain boundaries the actual fluctuations in composition were considered too small to have any significance. In view of the fact that the temperature of measurement of the diffusion coefficient was close to the melting point of the alloy, and as the grain size was of the order of 0·3 to 0·4 cm. it was thought that enhanced grain boundary diffusion would be negligable. The sample surface was ground flat on SiC paper and a layer of radioactive tracer plated on to the surface; the diffusion coefficient and solubility were then measured using the method outlined in Chapter 4. The results obtained are outlined in section 6.4.

6.3 Measurement of Interfacial Energy

In order to arrive at an estimate of the change in radius of the dispersoid with time from the Lifshitz-Wagner equation it was necessary to know the value of the solid-solid interfacial energy between the alloy and thoria. As a direct measurement of γ is difficult it was decided to measure the interfacial energy between liquid alloy and solid thoria and from this value it is possible to estimate the solid-solid value. Since the values of γ for $ThO_{2(solid)}$ - $H_{2(gas)}$ and Ni $alloy_{(liquid)}$ - $H_{2(gas)}$ are known it is possible to calculate γ $alloy_{(liquid)}$ - $ThO_{2(solid)}$ interface from the angle of contact of a sessile drop of alloy on a plane surface of thoria.

A pellet of pure ThO_2 with zero porosity was ground flat on SiC paper and diamond paste (finest paste 0·25 micron) to give a plane smooth surface. The pellet was then put into an alumina crucible and a small quantity of the alloy was then placed in the centre of the disc and the crucible put into the furnace (for details see Fig. 4). As the sample suspension contained one hook type linkage it was assumed that as the crucible would hang freely and, as it was loaded uniformly, the thoria disc would give a plane horizontal surface so that the sessile drop would be

symmetrical. Pure dry hydrogen ($PO_2 = 10^{-18}$atm.) was passed over the sample and the furnace heated up to 1550°C. and held at that temperature for one hour to allow equilibration of the sample with the furnace gas. The sample was then allowed to cool slowly so that the contact angle would be that of the alloy at its melting point. When the sample was cold the drop was then removed from the plaque. It was noticed that although the thoria pellet was slightly discoloured where the pellet had been, there was no other indication of interaction. The surface of the alloy was bright and shiny and there was no visible trace of any oxide layer present. The diameter of the pellet was then measured and the alloy drop was then mounted in a thermo-setting plastic and the pellet and mount ground on SiC paper until the diameter of the pellet had been reached. Photographs were then taken of the edges of the sample on a metallurgical microscope and from the film produced prints were made and from these prints the angle of contact measured.

Two different samples were treated in this manner which gave four readings for the angle of contact.

6.4 Results

6.4 (a) Interfacial energy

For a sessile drop the interfacial energy between the liquid drop and the solid substrate is defined by

$$\gamma_{(\text{solid-liquid})} = \gamma_{(\text{solid-gas})} - \cos\theta . \gamma_{(\text{liquid-gas})}$$

Where θ is the angle of contact between drop and substrate.

Sample No.	Contact Angle
1	114°
1	117°
2	115°
2	118·5°
Mean	116·1° (∓1·9°)

Values of $\gamma_{(\text{gas-liquid})}$

$Ni\text{-}H_2$ = 1768 ergs cm^{-2} (Ref: 46)

$Ni\text{-}10\%Cr\text{-}H_2$ = 1755 ergs cm^{-2} (Ref: 47)

Values of $\gamma_{(ThO_2 \text{solid} - H_2)}$ at 1500°C.

= 927 ergs cm^{-2} (Ref: 46)

= 595 ergs cm^{-2} (Ref: 47)

As can be seen the effect of an addition of 10% Cr to Ni results in a very small reduction in the interfacial energy. This could be explained in terms of the negative

departure from ideality of the alloy so an estimate of a value of δ 80% Ni - 10% Cr - 10% Pt = 1750 ergs cm^{-2} would appear reasonable. The two values for δ (ThO_2 solid - H_2) appear at variance and an average value of δ (ThO_2 solid - H_2) = 760 ergs cm^{-2} has been taken.

The above values give a value of the interfacial energy between 10% Ni - 10% Cr - 10% Pt (liquid) and ThO_2 (solid) of 1600 ($\pm$160) ergs cm^{-2}.

6.4 (b) Solubility and Diffusion of Th

Sample No. 30 80% Ni - 10% Cr - 10% Pt.

$PO_2 = 10^{-18}$ Atm. Anneal time = 6.45×10^4 sec.

Channel No.	Channel Counts	t*	$\times 10^{14}$ D_2 $cm^2 sec^{-1}$
6	490	1·393	6·13
7	400	1·452	6·22
8	341	1·499	6·79
9	283	1·552	7·05
10	234	1·602	7·61
11	192	1·656	7·78
12	156	1·711	7·34
		Mean D	6·99

Regression Coefficient = 0·9997

Intercept = 1·0819

$Co/_2$ = 1260 counts

Sample Area = 0·503 cm^2

Counting time = 7.2×10^4 sec

Co* = 1.75×10^{-2} counts sec^{-1}

Solubility = 2.82×10^{-2} Wt. %

Diffusion Coefficient = $6.99 (\mp 0.85) \times 10^{-14}$ $cm^2 sec^{-1}$

CHAPTER 7

DISCUSSION

7.1 Errors Involved in Measurement of Growth Rates

In considering the Lifshitz-Wagner equation the errors involved in the measurements of growth rates depend on the accuracy with which D, Co and r^{-3} can be measured.

The variation in the values of D are quoted in the results tables. These errors are due to a number of factors. The main source of error is the presence of Th^{232} in the plating solution. As was stated in section 4.5 the relative energies of Th^{230} and Th^{232} are 4·68 MeV and 4·01 MeV respectively, hence there is an increase in the counts in channels 9 to 13 due to the lower energy particles. Although some of these counts are removed from the measured counts with the background correction, there still remains some counts which give a scatter to the points of the channel number vs. t* graph, this leads to a decrease in the linearity of the graph. Another source of error is the low number of counts recorded in each channel. As the error in the count for a radio-active decay is proportional to the square root of the number of counts, and as the number of counts varied from 1000 to 100 the error varies from 3% at 1000 counts to 10% at 100 counts.

The errors shown on the results tables and graphs of diffusion coefficients were deduced from the maximum and minimum values of D calculated for all channels; it must be noted that in some cases the fluctuation of the value of D is not random with channel number, but that channels 6, 7, 14 and 15 give high values whereas other channels give low values. The possible explanation for this effect is that channels 6 and 7 were still influenced by the mis-sorting of the counts from the surface layer (see section 4.6). The deviation in channels 14 and 15 is less easy to explain and a cause of this variation could be the extremely low number of counts recorded in these channels.

The reasons for the errors involved in the determination of Co are similar to those stated above for the evaluation of D. Co is found using the intercept of the graph of t* vs. channel number, and the scatter in channel counts from a straight line gives rise to errors in the intercept. In all the results tables a value of the correlation coefficient of regression is quoted, as this value is an indication of the linearity of the graph, it can be used to assess the accuracy of the value of the planar interfacial solubility which was calculated.

As described in section 4.2, the samples used for the determination of diffusion coefficients were annealed at 1350°C. for twenty hours before plating, this treatment gave grain sizes of the order of 0·1 cm. Using this value as the diameter of a spherical grain this gave a total grain boundary length of the order of 20 cms. for a 2 cm^2 sample area. If we assume the thickness of a boundary as 3 atomic layers, i.e. about 10 Angstroms, this gives a total grain boundary vol. of 2×10^{-6} cm^3. As the grain boundary diffusion coefficient is usually a factor of 10^4 greater than that for the bulk material, and we assume saturation of the grain boundaries after solution treatment, the count due to the grain boundaries will be 10^{-6} of the interfacial solubility count. This count was usually a 1000 to 3000 counts so the effect of grain boundary diffusion is seen to be negligable.

The errors involved in the measurement of the mean radius of the thoria particles are mainly due to the fact that there is a wide range of particle sizes in each sample. As can be seen from the histograms the variation of particle diameter with percentage of total number is of the form of a Poisson distribution, with a correlation coefficient of approximately 80%. Because of this type of

distribution we can use the fact that the mean of a Poisson distribution is equal to its variance hence the errors involved in the evaluation of $\bar{r}^3$ can be simply stated as the square root of $\bar{r}$ equals the standard deviation. In the graphs of $\bar{r}^3$ vs. time each value of the mean radius is shown plus or minus one standard deviation. The only other source of error in the measurement of $\bar{r}$ comes from the calibration of the electron microscope or any loss in accuracy during the process of photographic enlargement, but since the errors from the electron microscope magnification are very small and film shrinkage is eliminated using glass plates, these errors can be ignored in light of the 7 to 5 percent inaccuracy in the value of $\bar{r}$ due to the distribution.

The errors involved in the evaluation of the slope of the graph $\bar{r}^3$ vs. time are negligable in the case of growth under oxygen partial pressures of 10^{-8}atm. and 10^{-14}atm. However, in the case of PO_2 equals 10^{-18}atm. there is a very wide scatter of the points around the best straight line found from linear regression analysis. This scatter is reflected in a correlation coefficient of 0·7233 and the slope of the line leads to an interfacial

energy of ThO_2 - Ni of 4505 erg cm^{-2}. Also shown on the graph is a line which would give a value of the interfacial energy of 2000 erg cm^{-2} and as can be seen both lines would appear equally likely in view of the uncertainty of the points. The reason for this scatter of points is hard to ascertain as all the experimental conditions used would produce similar errors; the only difference between experiments for the determination of growth rates under a PO_2 of 10^{-18}atm. and the other growth rate determinations was that the samples were cut from different sheets of T. D. Nickel which could possibly have had different thermal treatments in manufacture.

In view of the long treatment times (up to 400 hours) any error incurred due to growth during heating up or cooling down of the samples can be considered negligable and the treatment times were taken as starting from the instant that the furnace reached temperature and ending when the furnace was switched off. The treatment temperature was found using a Pt/Pt 13% Rh thermocouple the output of which was measured on a potentiometer, so any variation in temperature was due to the accuracy of the furnace controller which was stated as $\mp$ 2 degrees.

7.2 Discussion of Results Obtained for the Growth Rates of ThO_2 in Nickel

As was outlined in section 1.3 it was hoped to test the applicability of the Lifshitz-Wagner equation to the Ni - ThO_2 system, the equation implies one basic assumption that is; there exists an equilibrium between the particle and its immediate environment and therefore the growth is controlled by the diffusion of the slowest moving dispersoid component through the matrix. The difference between growth rate equations for interface and diffusion control is the power to which the mean radius is raised. In interface control the growth rate equation shows a linear dependance between $\bar{r}^2$ and time whereas in diffusion controlled growth $\bar{r}^3$ is proportional to time. The graphs of $\bar{r}^3$ vs. time are of a linear form with correlation coefficients of better than 0·99 which means that the assumption of diffusion controlled growth for the Ni - ThO_2 system is a valid one, and means that if the appropriate values of the diffusion coefficient and solubility at a plane interface are substituted into the Lifshitz-Wagner growth rate equation we can arrive at a value for the interfacial energy between solid ThO_2 and solid Ni.

For growth of ThO_2 at 1350°C. under an oxygen partial pressure of 10^{-8}atm. the value calculated was 2030 (∓1100) ergs cm^{-2} and at 1350°C. under a partial pressure of 10^{-14}atm. the value was 1590 (∓880) erg cm^{-2}. As there are no accurately known measurements of the solid-solid interfacial energy for the Ni - ThO_2 system the only comparison that can be made with other results is with the $Ni_{(liquid)}$ - $ThO_{2\ (solid)}$ system. Humenick and Kingery [46] measured the interfacial energy between Ni and ThO_2 using a sessile drop technique and the values they quote are:-

$$\gamma_{Ni - ThO_2} = 1540 \text{ erg cm}^{-2}$$

at 1500°C. under dry hydrogen and

$$\gamma_{Ni - ThO_2} = 1520 \text{ erg cm}^{-2}$$

at 1500°C. under dry helium.

Armstrong, Chacklader and Clarke [47] also measured this interfacial energy using a sessile drop at 1500°C. under dry hydrogen and their value was 1500 erg cm^{-2}. There is some difficulty in assessing the difference between solid-solid and solid-liquid as the interfacial energies of solid-solid systems are rarely evaluated. However, Udin and Wulff [48] have measured γ for solid

silver and solid gold and comparison of their results with the values for a liquid system it would appear that the solid-solid interfacial energy is 25% greater than the solid liquid system. Applying this criterium to the results obtained from the experiments mentioned above we arrive at a value of 1620 erg cm^{-2} for an oxygen partial pressure of 10^{-8}atm. and 1272 erg cm^{-2} for an oxygen partial pressure of 10^{-14}atm.

These results compare favourably with the values obtained by Humenick and Kingery and in view of the linearity of the mean radius cubed versus treatment time graphs, it would seem reasonable to conclude that the growth of a thoria dispersoid in pure nickel is an example of diffusion controlled Ostwald ripening as described by the Lifshitz-Wagner equation.

7.3 Discussion of Errors involved in the Measurement of D_{Th} and Co_{Th} in Ni - Cr alloys

The errors involved in the determination of the diffusion coefficients and the equilibrium interfacial solubility of Th in Ni-Cr alloys are identical with the errors outlined in section 7.1 for pure nickel; the only difference between the two experimental procedures

being that oxygen partial pressure at which the determinations were carried out, as in order to prevent the formation of Cr_2O_3 on the Ni-Cr alloy surface the treatment gas has to have a PO_2 of 10^{-18}atm. or less. Since the gas used was pure dry hydrogen this condition was achieved and no visible trace of oxide was found.

7.4 Discussion of Results for Th Solubility and Diffusion in Ni - Cr

The heat treatment prior to the diffusion anneal given to these samples was identical to that described in section 7.1 and the grain sizes achieved were of the same order. Despite this, it was found that in some cases the value of D calculated varied with treatment time in a manner which indicated that equilibrium had not been reached at the interface until the samples had been treated for times in excess of 16 hours. This effect is shown in the results tabulated in the appendix where, for example sample no. 19 which was annealed for $7{\cdot}9 \times 10^4$ sec gives a much higher value of D than samples no. 18 and 17 which give the same value after treatment times of $14{\cdot}94 \times 10^4$ sec and $21{\cdot}43 \times 10^4$ sec respectively. A similar trend is shown in the 5% results, the results for Ni- 10% Cr also show the same trend. However, in the case of the

Ni - 15% Cr samples, one sample (No. 26) that was treated for only $7 \cdot 59 \times 10^4$ sec gave the same value as sample no. 27 - 28 which required a much longer time ($10 \cdot 71 \times 10^4$ sec) to reach this value; the reason for this variation is not known since the samples were cut from the same strip of material and had identical treatment prior to the diffusion anneal. The Ni - 20% Cr alloy was only heated for $7 \cdot 16 \times 10^4$sec as after this time it produced a value for the diffusion coefficient which would appear reasonable with regard to the other results, and the significance of this result is limited because of the possibility of super-lattice formation.

The results for the solubility which are quoted in the results tables show a large variation from sample to sample of the same composition, although the trend due to non-equilibration at the interface is the same as in the case of the diffusion coefficient. At first, this fluctuation would appear at variance with the accuracies shown in the summary table on page 71, but it must be realised that the errors quoted are those arising from the linear regression analysis; for this reason no error limits are shown on Fig. 12 as the scatter in the points would indicate a greater error, such as that found

between a number of samples .

It was thought that the solubility of Th would increase if chromium was added to the nickel owing to the alteration of the Th:O_2 balance in the lattice (see section 1.5) however, the results are too imprecise to indicate any definite variation of the solubility. The reason for this lack of change is thought to be due to the extremely low oxygen partial pressure under which the experiments were carried out as at a PO_2 of 10^{-18}atm. the concentration of oxygen in the lattice is so low (approximately 10^{-5}atms. cm^{-3}) it becomes negligable when compared to other imperfections such as dislocations (equilibrium concentration approximately 10^{8} cm^{-3}).

The diffusion coefficient of thorium in nickel - chromium shows a 100% increase from pure Ni to Ni- 20% Cr in an approximately linear manner, once again it was thought that as the oxygen partial pressure was so low the effect of inter-stitial oxygen was negligable and that the increase in the diffusion coefficient was due to an increase in the disorder in the lattice caused by the chromium ions, which would decrease the activation energy for the diffusion process and also alter the

pre-exponential term as outlined by Seitz [49].

7.5 Discussion of the Ni-Cr-Pt Results

The value of interfacial energy found appears consistent with the premise that small additions of alloying elements to nickel do not cause a large varation from the value for pure nickel; this being explained by the fact that both chromium and platinum show negative departures from ideal solution behaviour in nickel. The decrease in the solubility of Th with the addition of Pt to a Ni- 10% Cr alloy is of doubtful significance bearing in mind the uncertainty shown in the other solubility determinations. However, if there is any variation it would appear that the addition of platinum to this alloy decreases the solubility slightly. The diffusion coefficient of Th is increased 100% with the addition of platinum at this alloy composition and the reason for this is thought to be the same as that in the case of chromium additions to nickel.

7.6 Conclusions

The general conclusions from this study are that

(1) The growth of thoria particles in T. D. Nickel is a diffusion controlled process as described by the Lifshitz-Wagner equation.

(2) The addition of chromium to nickel increases the diffusion coefficient of thorium by up to 100% in a Ni - 20% Cr alloy.

(3) There appears little increase of the equilibrium inferfacial solubility of Th in Ni over the range 0 to 20% Cr.

(4) The growth of thoria particles in T. D. Ni - 20% Cr would be twice as fast as in pure Ni at 1350°C. under a PO_2 of 10^{-18}atm.

(5) The effect of the addition of 10% platinum to a Ni - 10% Cr alloy would be to increase the growth rate 50% over the rate for a Ni-10% Cr alloy at 1350°C. and a PO_2 of 10^{-18}atm.

APPENDIX

TABLE 1

Equivalent Depth Versus Channel Number

Channel Number from Surface	Depth in Microns in Nickel
1	0·123
2	0·250
3	0·379
4	0·510
5	0·639
6	0·769
7	0·900
8	1·031
9	1·159
10	1·289
11	1·417
12	1·543
13	1·668
14	1·790
15	1·914

TABLE 2

Counts obtained from a monoenergetic source

Channel Number	Count
100	8
99	43
98	1,356
97	7,513
96	10,100
95	5,106
94	1,938
93	856
92	393
91	161
90	60
89	29
88	24
87	20
86	24
85	19
84	21
83	13
82	15
81	12
80	12

TABLE 3

Background Count for Instrument Using Unplated Nickel Sheet Sample

Channel Number	Count
80	208
79	197
78	181
77	159
76	137
75	115
74	95
73	80
72	67
71	62
70	57
69	42
68	35
67	30
66	26
65	23

SAMPLE NO. 1 As received (1)

Diameter Interval (A)	No. Of Particles	% Of Total
0 - 50	6	1·60
50 - 100	22	6·10
100 - 150	42	11·57
150 - 200	43	11·85
200 - 250	34	9·36
250 - 300	26	7·16
300 - 350	39	10·74
350 - 400	30	8·26
400 - 450	20	5·51
450 - 500	10	2·75
500 - 550	19	5·23
550 - 600	13	3·58
600 - 650	7	1·93
650 - 700	10	2·75
700 - 750	3	0·83
750 - 800	10	2·75
800 - 850	3	0·83
850 - 900	2	0·55
900 - 950	6	1·60
950 - 1000	3	0·83
1000 - 1050	5	1·38
1050 - 1100	2	0·55
1100 - 1150	0	0·00
>1150	8	2·21
TOTAL NO.	363	

Mean radius = 176·1 A $\bar{r}^3 = 5{\cdot}46 \times 10^{-18} cm^3$

SAMPLE NO. 2 As received (2)

Diameter Interval (A)	No. Of Particles	% Of Total
0 - 50	0	0·00
50 - 100	2	0·94
100 - 150	9	4·25
150 - 200	13	6·13
200 - 250	21	9·90
250 - 300	15	7·08
300 - 350	15	7·08
350 - 400	16	7·55
400 - 450	14	6·60
450 - 500	21	9·90
500 - 550	17	8·02
550 - 600	12	5·66
600 - 650	6	2·83
650 - 700	6	2·83
700 - 750	8	3·77
750 - 800	9	4·25
800 - 850	7	3·30
850 - 900	3	1·42
900 - 950	3	1·42
950 - 1000	5	2·36
1000 - 1050	7	3·30
1050 - 1100	0	0·00
>1100	3	1·42
TOTAL NO.	212	

Mean radius = 240·2 A $\bar{r}^3 = 13{\cdot}86 \times 10^{-18}\,cm^3$

SAMPLE NO. 3 50 Hours with oxide on surface

Diameter Interval (A)	No. Of Particles	% Of Total
0 - 50	1	0·75
50 - 100	2	1·50
100 - 150	8	6·02
150 - 200	6	4·51
200 - 250	11	8·27
250 - 300	11	8·27
300 - 350	12	9·02
350 - 400	15	11·28
400 - 450	5	3·76
450 - 500	3	2·26
500 - 550	6	4·51
550 - 600	9	6·77
600 - 650	6	4·51
650 - 700	6	4·51
700 - 750	3	2·26
750 - 800	4	3·00
800 - 850	4	3·00
850 - 900	4	3·00
900 - 950	1	0·75
950 - 1000	2	1·50
1000 - 1050	3	2·26
1050 - 1100	2	1·50
>1100	10	7·52
	TOTAL NO. 133	

Mean radius = 266·0 A $\bar{r}^3 = 18{\cdot}82 \times 10^{-18} cm^3$

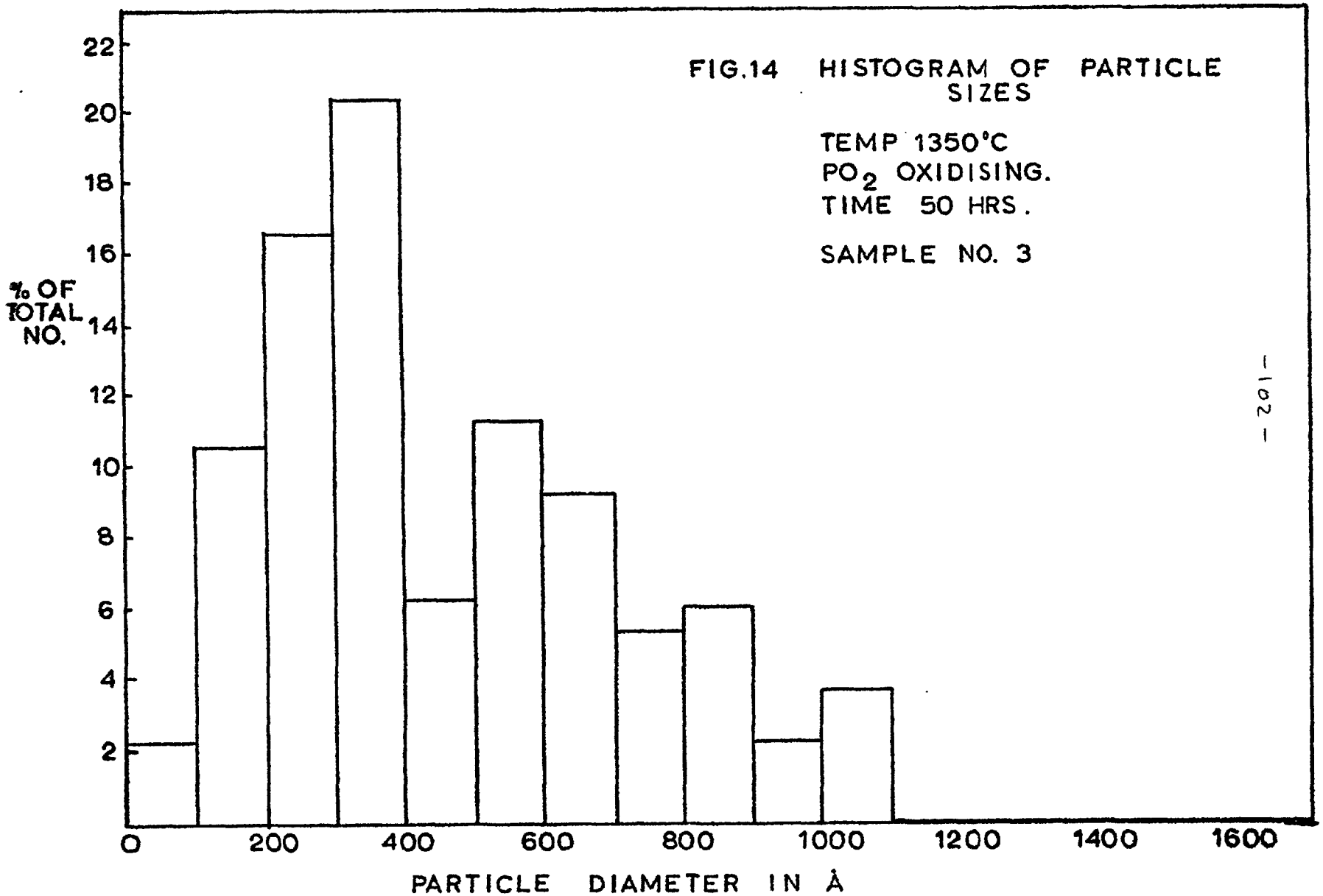
FIG.14 HISTOGRAM OF PARTICLE SIZES
TEMP 1350°C
PO_2 OXIDISING.
TIME 50 HRS.
SAMPLE NO. 3
% OF TOTAL NO.
22
20
18
16
14
12
10
8
6
4
2
0
200
400
600
800
1000
1200
1400
1600
PARTICLE DIAMETER IN Å

SAMPLE NO. 4 100 Hours with oxide on surface

Diameter Interval (A)	No. Of Particles	% Of Total
0 - 50	0	0·00
50 - 100	0	0·00
100 - 150	11	8·03
150 - 200	7	5·11
200 - 250	12	8·76
250 - 300	9	6·57
300 - 350	11	8·03
350 - 400	17	12·41
400 - 450	9	6·57
450 - 500	5	3·65
500 - 550	11	8·03
550 - 600	6	4·38
600 - 650	6	4·38
650 - 700	10	7·30
700 - 750	5	3·65
750 - 800	1	0·73
800 - 850	4	2·92
850 - 900	2	1·46
900 - 950	1	0·73
950 -1000	0	0·00
1000 -1050	2	1·46
1050 -1100	3	2·19
>1100	5	3·65
TOTAL NO.	137	

Mean radius = 244·5 A $\bar{r}^3 = 14{\cdot}612 \times 10^{-18} cm^3$

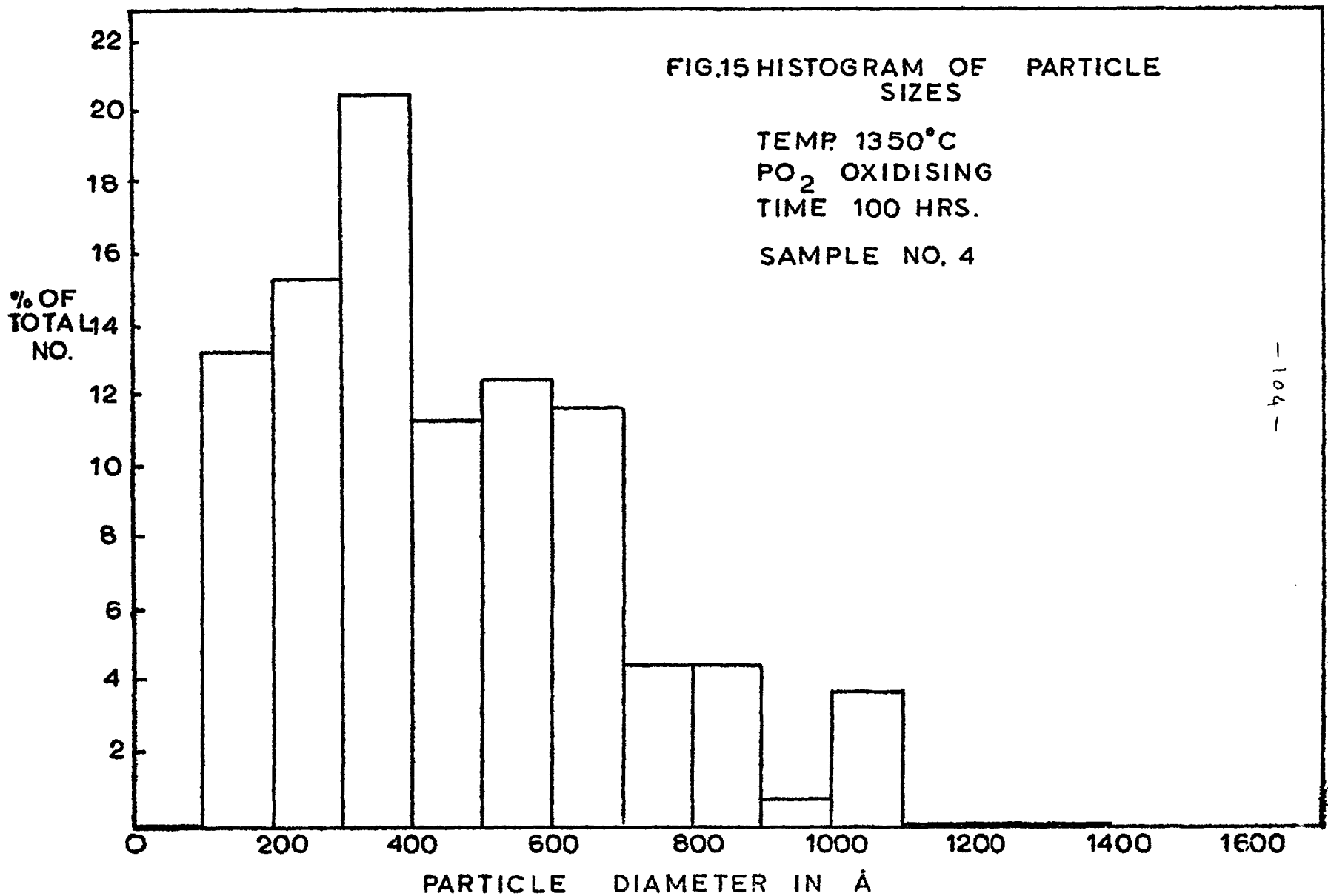
FIG.15 HISTOGRAM OF PARTICLE SIZES
TEMP. 1350°C
PO_2 OXIDISING
TIME 100 HRS.
SAMPLE NO. 4
% OF TOTAL NO.
22
20
18
16
14
12
10
8
6
4
2
0
200
400
600
800
1000
1200
1400
1600
PARTICLE DIAMETER IN Å

SAMPLE NO. 5 50 Hours at $PO_2 = 10^{-8}$ atm.

Diameter Interval (A)	No. Of Particles	% Of Total
0 - 50	2	1•22
50 - 100	2	1•22
100 - 150	8	4•88
150 - 200	8	4•88
200 - 250	12	7•32
250 - 300	10	6•10
300 - 350	11	6•71
350 - 400	11	6•71
400 - 450	13	7•93
450 - 500	13	7•93
500 - 550	9	5•49
550 - 600	11	6•71
600 - 650	9	5•49
650 - 700	9	5•49
700 - 750	8	4•88
750 - 800	5	3•05
800 - 850	4	2•44
850 - 900	6	3•66
900 - 950	6	3•66
950 - 1000	0	0•00
1000 - 1050	0	0•00
1050 - 1100	1	0•61
1100 - 1150	1	0•61
>1150	5	3•05
TOTAL NO.	164	

Mean radius = 226•25 A $\bar{r}^3 = 11•58 \times 10^{-18} cm^3$

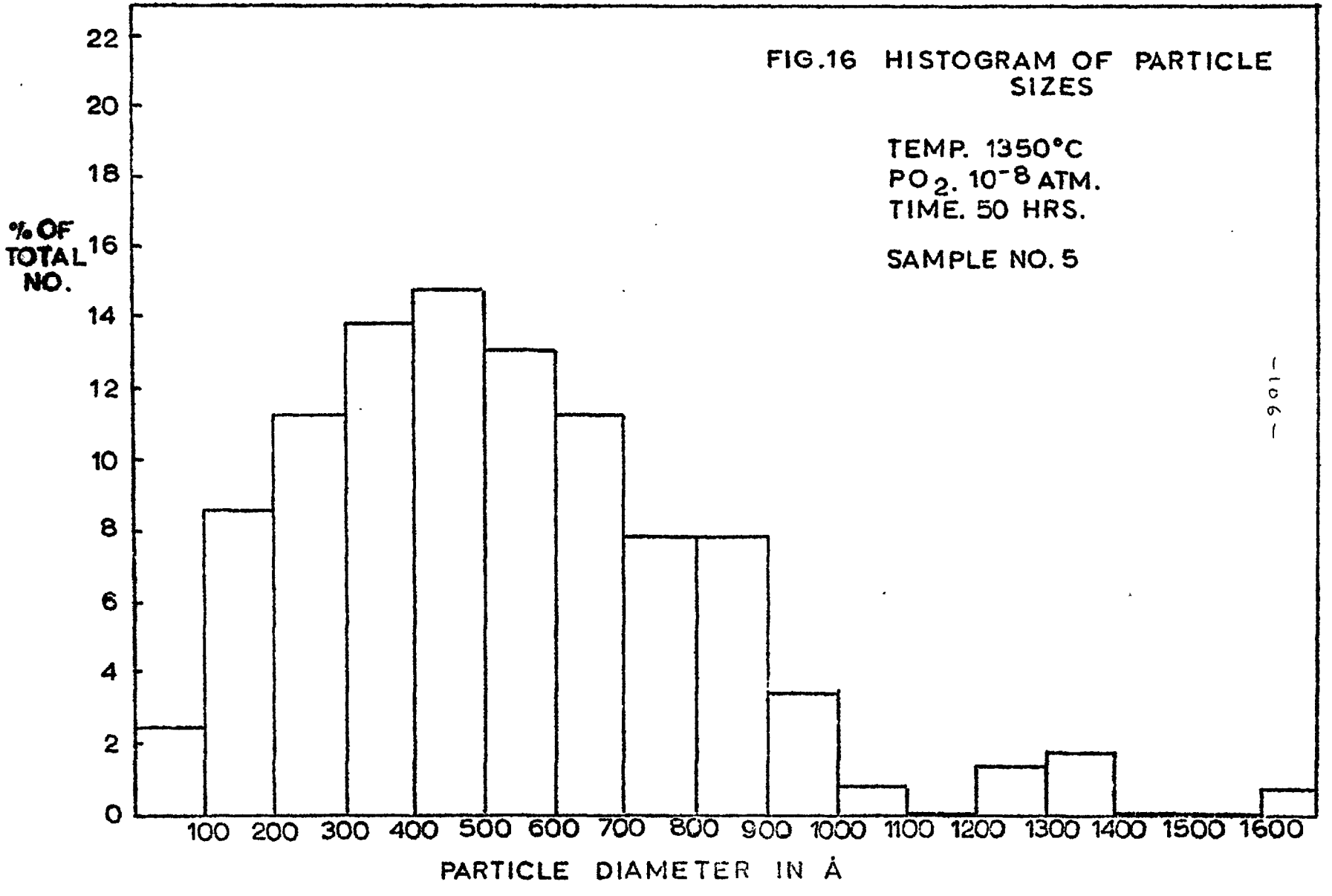
FIG.16 HISTOGRAM OF PARTICLE SIZES
TEMP. 1350°C
PO_2. 10^{-8} ATM.
TIME. 50 HRS.
SAMPLE NO. 5
% OF TOTAL NO.
0
2
4
6
8
10
12
14
16
18
20
22
100 200 300 400 500 600 700 800 900 1000 1100 1200 1300 1400 1500 1600
PARTICLE DIAMETER IN Å

SAMPLE NO. 6 100 Hours at $PO_2 = 10^{-8}$ atm.

Diameter Interval (A)	No. Of Particles	% Of Total
0 - 50	0	0·00
50 - 100	2	1·00
100 - 150	5	2·50
150 - 200	8	4·00
200 - 250	13	6·50
250 - 300	22	11·00
300 - 350	23	11·50
350 - 400	22	11·00
400 - 450	18	9·00
450 - 500	15	7·50
500 - 550	16	8·00
550 - 600	12	6·00
600 - 650	11	5·50
650 - 700	10	5·00
700 - 750	4	2·00
750 - 800	3	1·50
800 - 850	2	1·00
850 - 900	3	1·50
900 - 950	5	2·50
950 - 1000	2	1·00
1000 - 1050	2	1·00
1050 - 1100	1	0·50
>1100	1	0·50
TOTAL NO.	200	

Mean radius = 246·5 A $\bar{r}^3 = 14{\cdot}98 \times 10^{-18} cm^3$

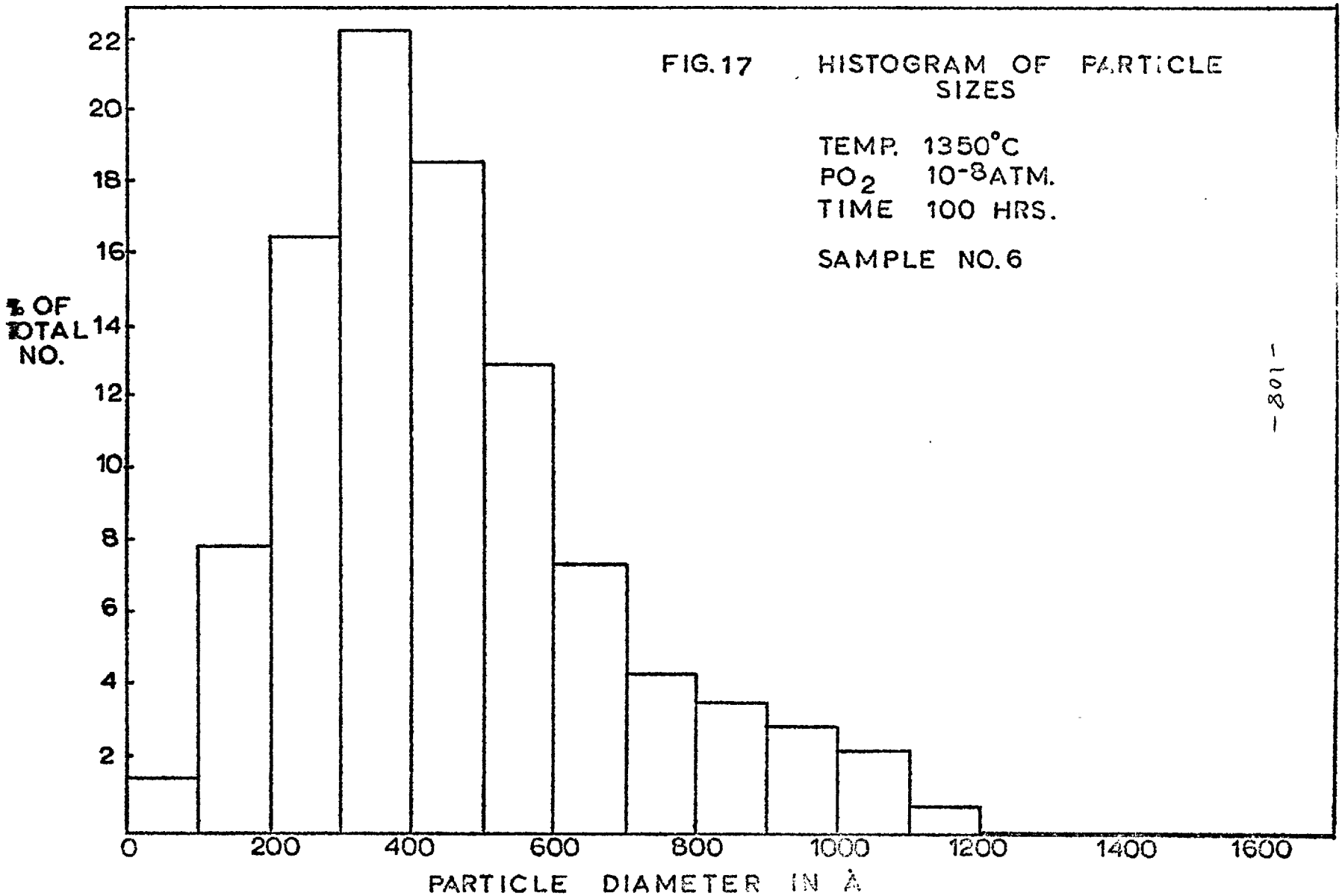
FIG. 17 HISTOGRAM OF PARTICLE SIZES
TEMP. 1350°C
PO_2 10^{-8} ATM.
TIME 100 HRS.
SAMPLE NO. 6
% OF TOTAL NO.
22
20
18
16
14
12
10
8
6
4
2
0
200
400
600
800
1000
1200
1400
1600
PARTICLE DIAMETER IN Å

SAMPLE NO. 7 200 Hours at $PO_2 = 10^{-8}$ atm.

Diameter Interval (A)	No. Of Particles	% Of Total
0 - 50	0	0
50 - 100	0	0
100 - 150	3	1·93
150 - 200	5	3·23
200 - 250	6	3·87
250 - 300	7	4·51
300 - 350	9	5·81
350 - 400	9	5·81
400 - 450	14	9·03
450 - 500	16	10·32
500 - 550	15	9·68
550 - 600	16	10·32
600 - 650	13	8·39
650 - 700	7	4·51
700 - 750	6	3·87
750 - 800	4	2·58
800 - 850	4	2·58
850 - 900	6	3·87
900 - 950	4	2·58
950 - 1000	1	0·64
1000 - 1050	2	1·28
1050 - 1100	2	1·28
1100 - 1150	1	0·64
1150 - 1200	0	0·00
>1200	5	3·23
	TOTAL NO. 155	

Mean radius = 282·0 A $\bar{r}^3 = 22{\cdot}43 \times 10^{-18}\ cm^3$

SAMPLE NO. 8 — 50 Hours at $PO_2 = 10^{-14}$ atm.

Diameter Interval (A)	No. Of Particles	% Of Total
0 - 50	0	0·00
50 - 100	9	3·00
100 - 150	15	5·00
150 - 200	24	8·00
200 - 250	34	11·33
250 - 300	41	13·67
300 - 350	32	10·67
350 - 400	29	9·67
400 - 450	26	8·67
450 - 500	18	6·00
500 - 550	15	5·00
550 - 600	13	4·33
600 - 650	9	3·00
650 - 700	8	2·67
700 - 750	7	2·33
750 - 800	6	2·00
800 - 850	6	2·00
850 - 900	3	1·00
900 - 950	0	0·00
950 - 1000	1	0·33
1000 - 1050	1	0·33
1050 - 1100	1	0·33
> 1100	2	0·67
	TOTAL NO. 300	

Mean radius = 198·5 A $\quad \bar{r}^3 = 7{\cdot}82 \times 10^{-18}\,cm^3$

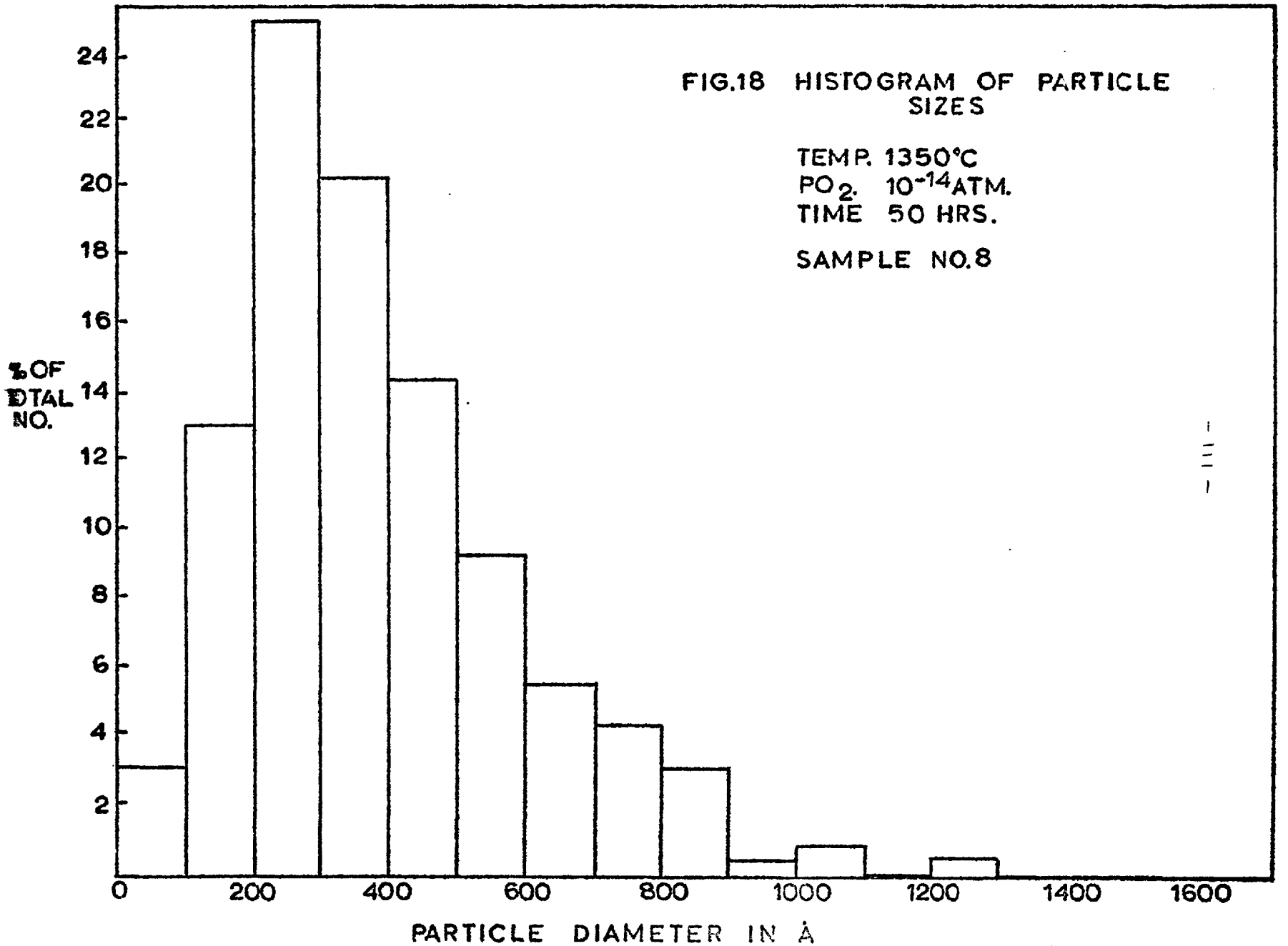
FIG.18 HISTOGRAM OF PARTICLE SIZES
TEMP. 1350°C
PO_2. 10^{-14}ATM.
TIME 50 HRS.
SAMPLE NO.8
% OF TOTAL NO.
24
22
20
18
16
14
12
10
8
6
4
2
0
200
400
600
800
1000
1200
1400
1600
PARTICLE DIAMETER IN Å

SAMPLE NO. 9 100 Hours at $PO_2 = 10^{-14}$ atm

Diameter Interval (A)	No. Of Particles	% Of Total
0 - 50	0	0·00
50 - 100	3	2·40
100 - 150	9	7·20
150 - 200	10	8·00
200 - 250	7	5·60
250 - 300	10	8·00
300 - 350	11	8·80
350 - 400	18	14·40
400 - 450	13	10·40
450 - 500	10	8·00
500 - 550	6	4·80
550 - 600	6	4·80
600 - 650	6	4·80
650 - 700	3	2·40
700 - 750	4	3·20
750 - 800	2	1·60
800 - 850	1	0·80
850 - 900	2	1·60
900 - 950	1	0·8
950 - 1000	2	1·60
1000 - 1050	1	0·80
>1100	0	0·00
TOTAL NO.	125	

Mean radius = 205·3 A $\bar{r}^3 = 8{\cdot}65 \times 10^{-18} cm^3$

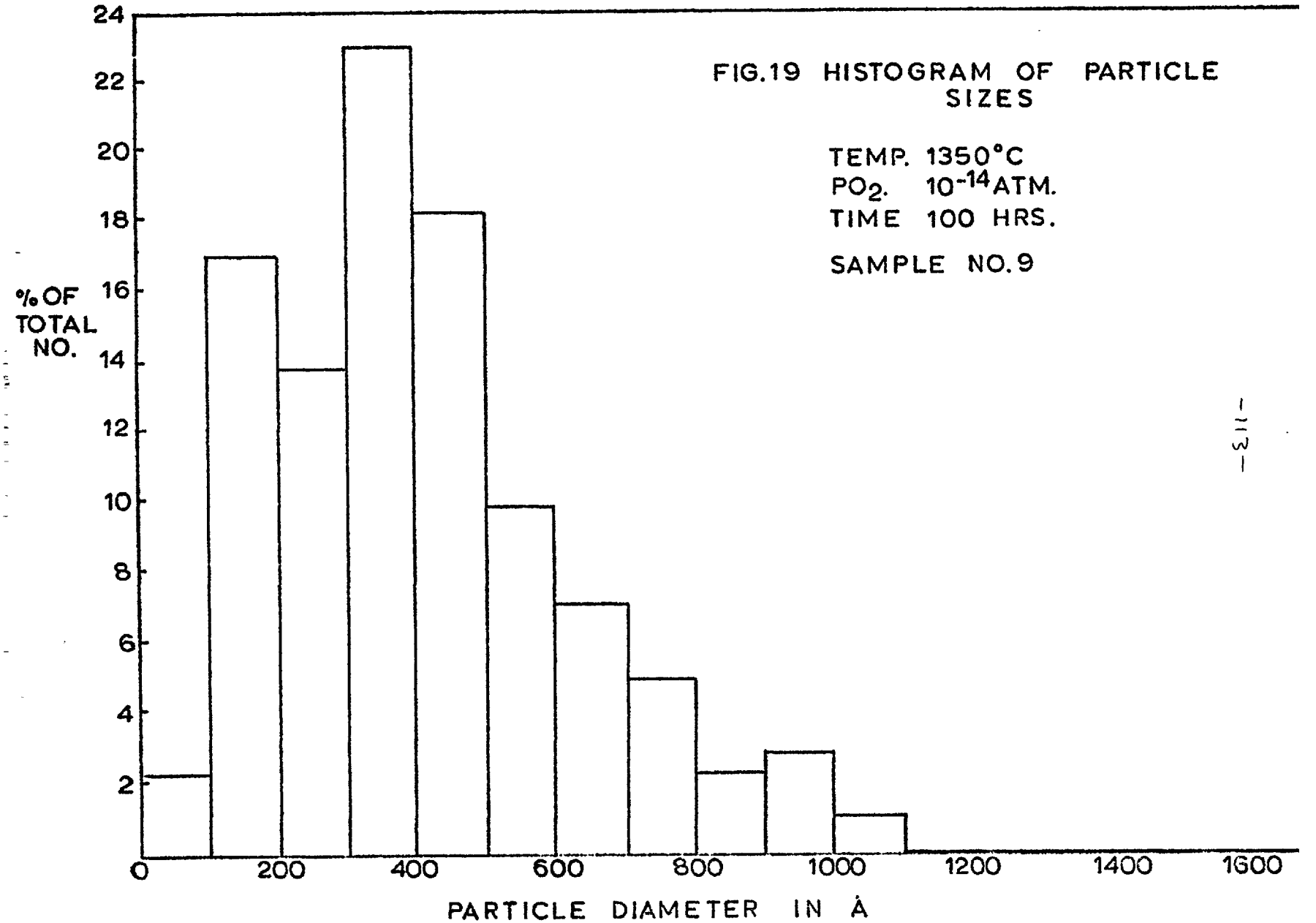

FIG.19 HISTOGRAM OF PARTICLE SIZES

TEMP. 1350°C
PO_2. 10^{-14} ATM.
TIME 100 HRS.

SAMPLE NO.9

SAMPLE NO. 10 200 Hours at $PO_2 = 10^{-14}$ atm.

Diameter Interval (A)	No. Of Particles	% Of Total
0 - 50	0	0·00
50 - 100	2	1·29
100 - 150	8	5·16
150 - 200	13	8·39
200 - 250	15	9·68
250 - 300	13	8·39
300 - 350	10	6·45
350 - 400	11	7·09
400 - 450	11	7·09
450 - 500	12	7·74
500 - 550	8	5·16
550 - 600	9	5·81
600 - 650	7	4·51
650 - 700	7	4·51
700 - 750	5	3·23
750 - 800	7	4·51
800 - 850	6	3·87
850 - 900	3	1·94
900 - 950	2	1·29
950 - 1000	3	1·94
1000 - 1050	1	0·65
1050 - 1100	2	1·29
1100 - 1150	0	0·00
>1150	1	0·65
TOTAL NO.	156	

Mean radius = 230·1 A $\bar{r}^3 = 12{\cdot}28 \times 10^{-18} cm^3$

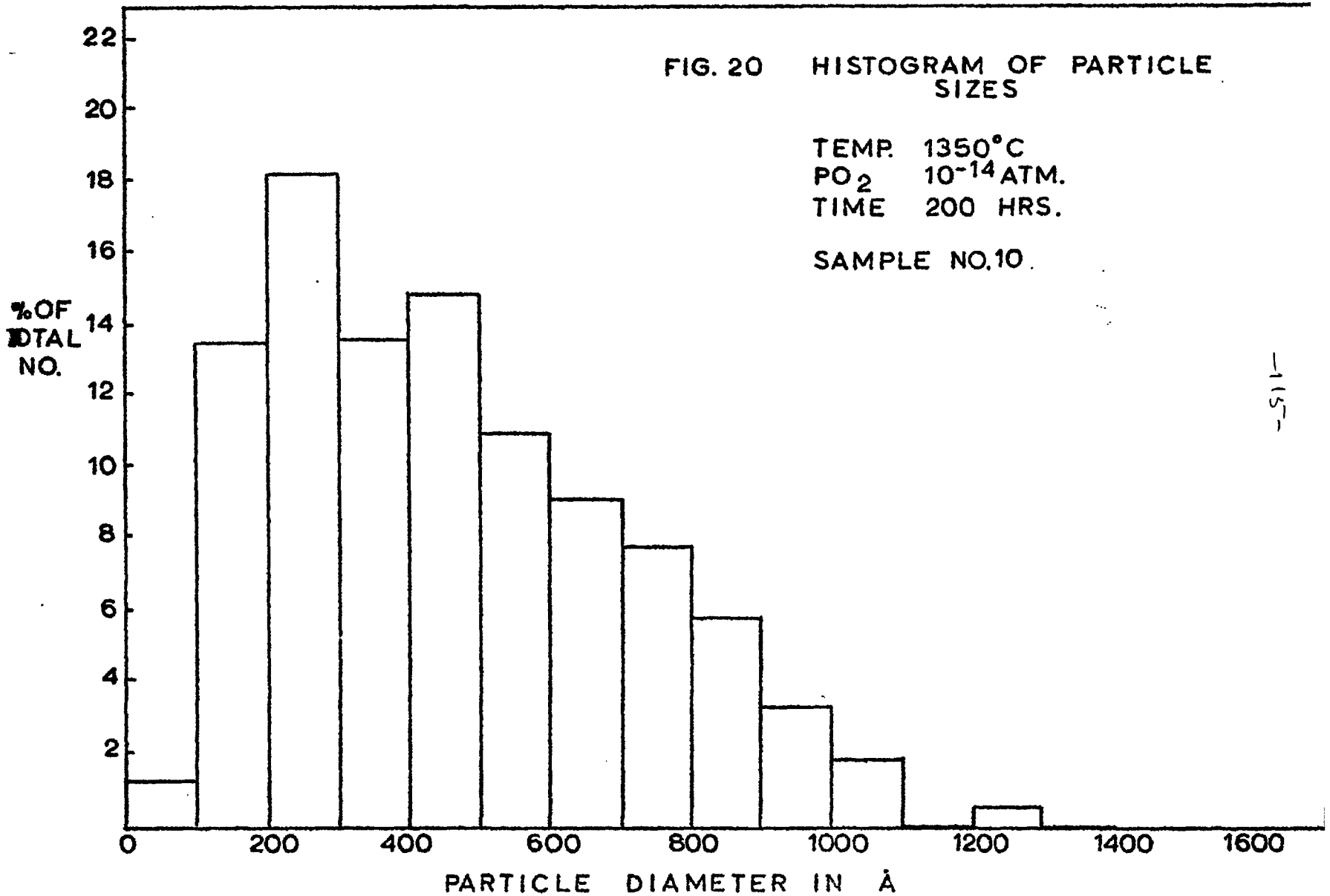
FIG. 20 HISTOGRAM OF PARTICLE SIZES
TEMP. 1350°C
PO2 10-14 ATM.
TIME 200 HRS.
SAMPLE NO.10
% OF TOTAL NO.
22
20
18
16
14
12
10
8
6
4
2
0
200
400
600
800
1000
1200
1400
1600
PARTICLE DIAMETER IN Å

SAMPLE NO. 11 100 Hours at $PO_2 = 10^{-18}$ atm.

Diameter Interval (A)	No. Of Particles	% Of Total
0 - 50	0	0·00
50 - 100	3	2·42
100 - 150	5	4·03
150 - 200	4	3·22
200 - 250	13	10·48
250 - 300	12	9·68
300 - 350	5	4·03
350 - 400	13	10·48
400 - 450	5	4·03
450 - 500	9	7·25
500 - 550	9	7·25
550 - 600	7	5·65
600 - 650	6	4·84
650 - 700	5	4·03
700 - 750	2	1·61
750 - 800	3	2·42
800 - 850	3	2·42
850 - 900	4	3·22
900 - 950	1	0·81
950 - 1000	3	2·42
1000 - 1050	3	2·42
1050 - 1100	1	0·81
>1100	8	6·45
TOTAL NO.	124	

Mean radius = 262·9 A $\bar{r}^3 = 18{\cdot}18 \times 10^{-18}\ cm^3$

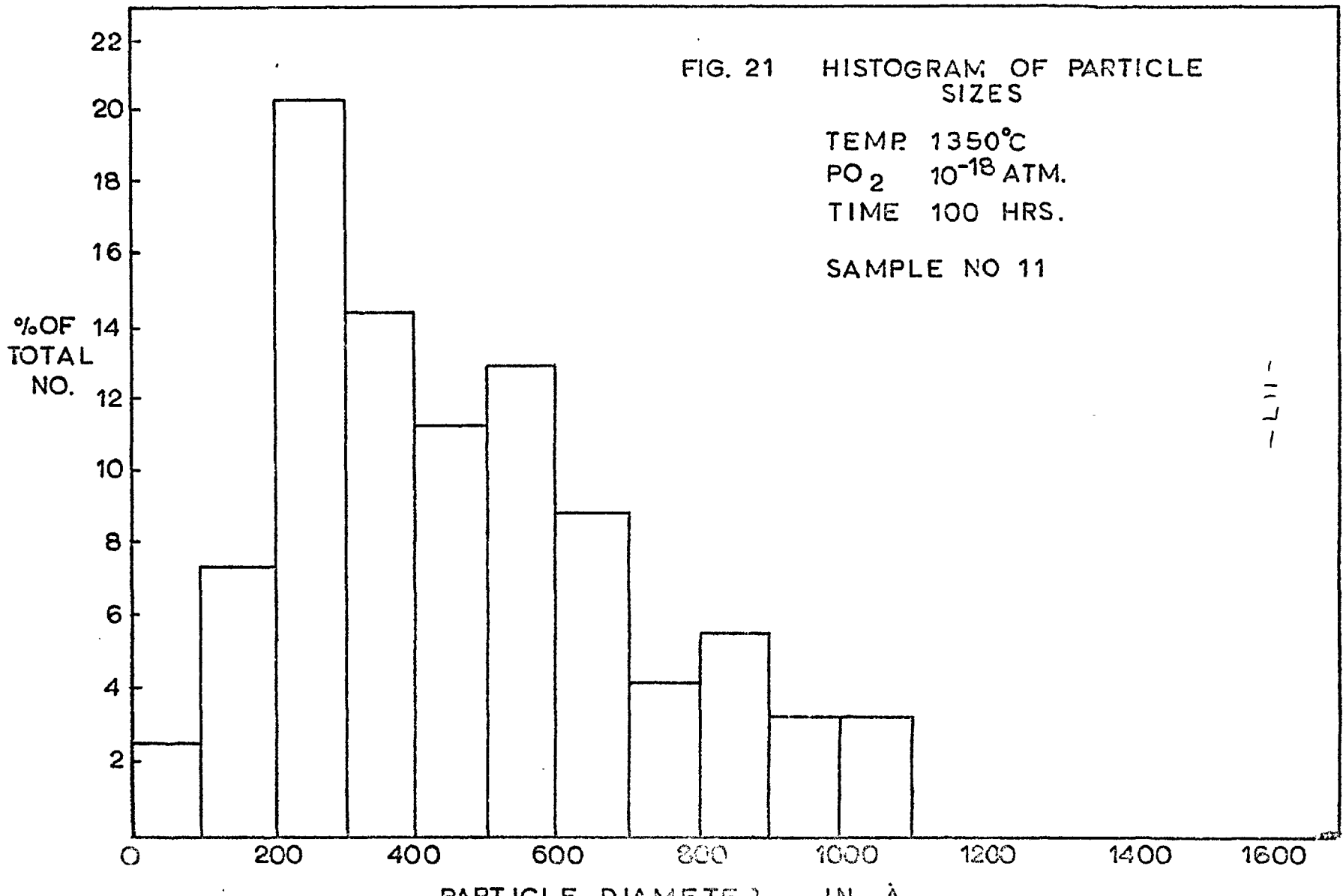
FIG. 21 HISTOGRAM OF PARTICLE SIZES
TEMP. 1350°C
PO_2 10^{-18} ATM.
TIME 100 HRS.
SAMPLE NO 11
%OF TOTAL NO.
22
20
18
16
14
12
10
8
6
4
2
0
200
400
600
800
1000
1200
1400
1600
PARTICLE DIAMETER IN Å

SAMPLE NO. 12 200 Hours at $PO_2 = 10^{-18}$ atm.

Diameter Interval (A)	No. Of Particles	% Of Total
0 - 50	0	0·00
50 - 100	1	0·63
100 - 150	2	1·27
150 - 200	7	4·43
200 - 250	18	11·39
250 - 300	11	6·96
300 - 350	18	11·39
350 - 400	17	10·76
400 - 450	6	3·80
450 - 500	10	6·33
500 - 550	9	5·70
550 - 600	7	4·43
600 - 650	13	8·22
650 - 700	8	5·06
700 - 750	1	0·63
750 - 800	4	2·53
800 - 850	1	0·63
850 - 900	7	4·43
900 - 950	3	1·90
950 - 1000	3	1·90
1000 - 1050	1	0·63
1050 - 1100	3	1·90
>1100	5	3·16
TOTAL NO.	158	

Mean radius = 2 51·5 A $\bar{r}^3 = 15{\cdot}90 \times 10^{-18} cm^3$

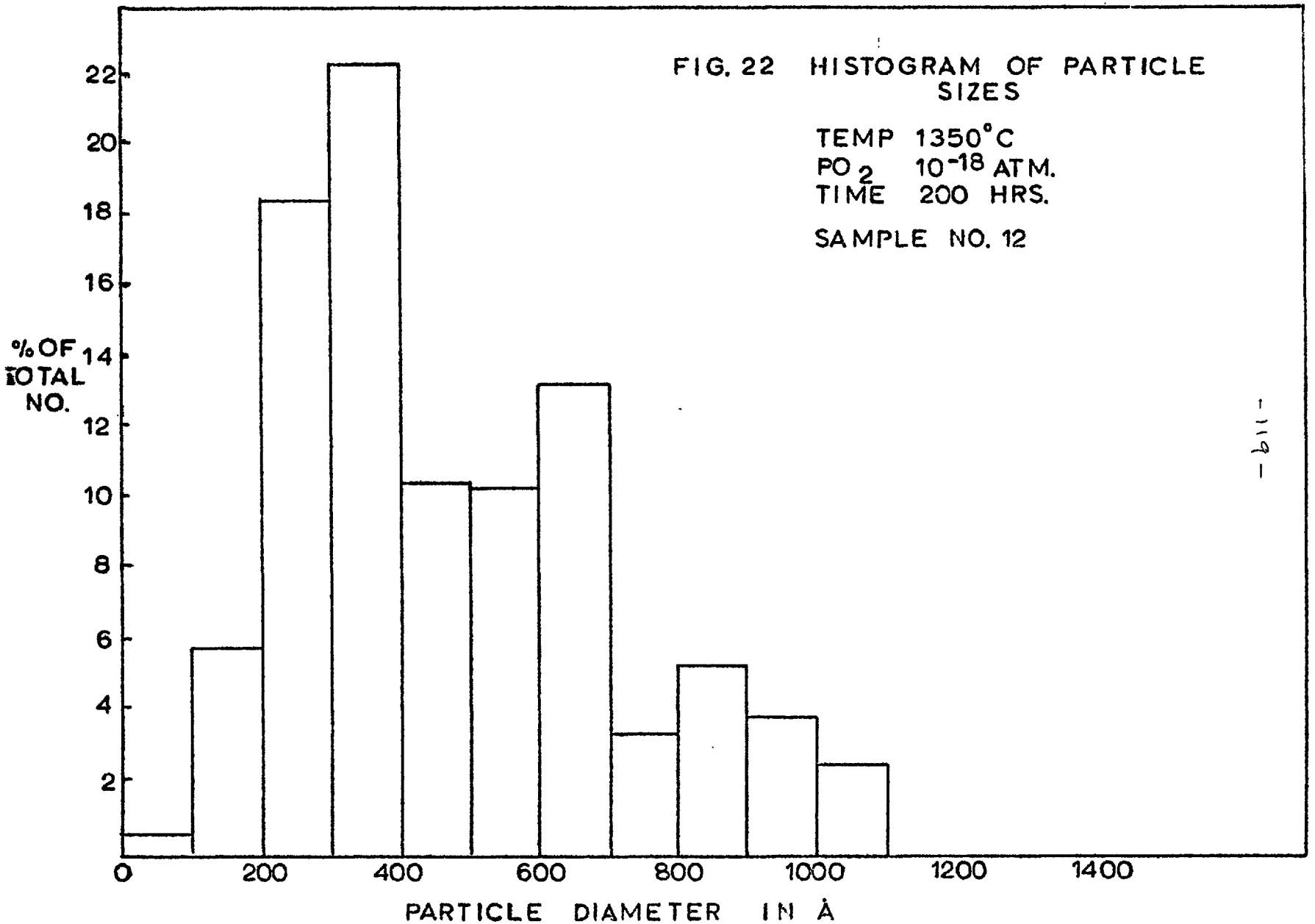
FIG. 22 HISTOGRAM OF PARTICLE SIZES
TEMP 1350°C
PO2 10-18 ATM.
TIME 200 HRS.
SAMPLE NO. 12
% OF TOTAL NO.
22
20
18
16
14
12
10
8
6
4
2
0
200
400
600
800
1000
1200
1400
PARTICLE DIAMETER IN Å

SAMPLE NO. 13 300 Hours at $PO_2 = 10^{-18}$ atm.

Diameter Interval (A)	No. Of Particles	% Of Total
0 - 50	0	0·00
50 - 100	2	1·90
100 - 150	1	0·95
150 - 200	6	5·71
200 - 250	10	9·52
250 - 300	8	7·62
300 - 350	9	8·57
350 - 400	9	8·57
400 - 450	10	9·52
450 - 500	7	6·66
500 - 550	8	7·62
550 - 600	8	7·62
600 - 650	5	4·76
650 - 700	3	2·86
700 - 750	6	5·71
750 - 800	4	3·81
800 - 850	2	1·90
850 - 900	2	1·90
900 - 950	2	1·90
950 - 1000	1	0·95
1000 - 1050	0	0·00
1050 - 1100	2	1·90
>1100	3	2·86
	TOTAL NO. 105	

Mean radius = 250·2 A $\bar{r}^3 = 15{\cdot}67 \times 10^{-18} cm^3$

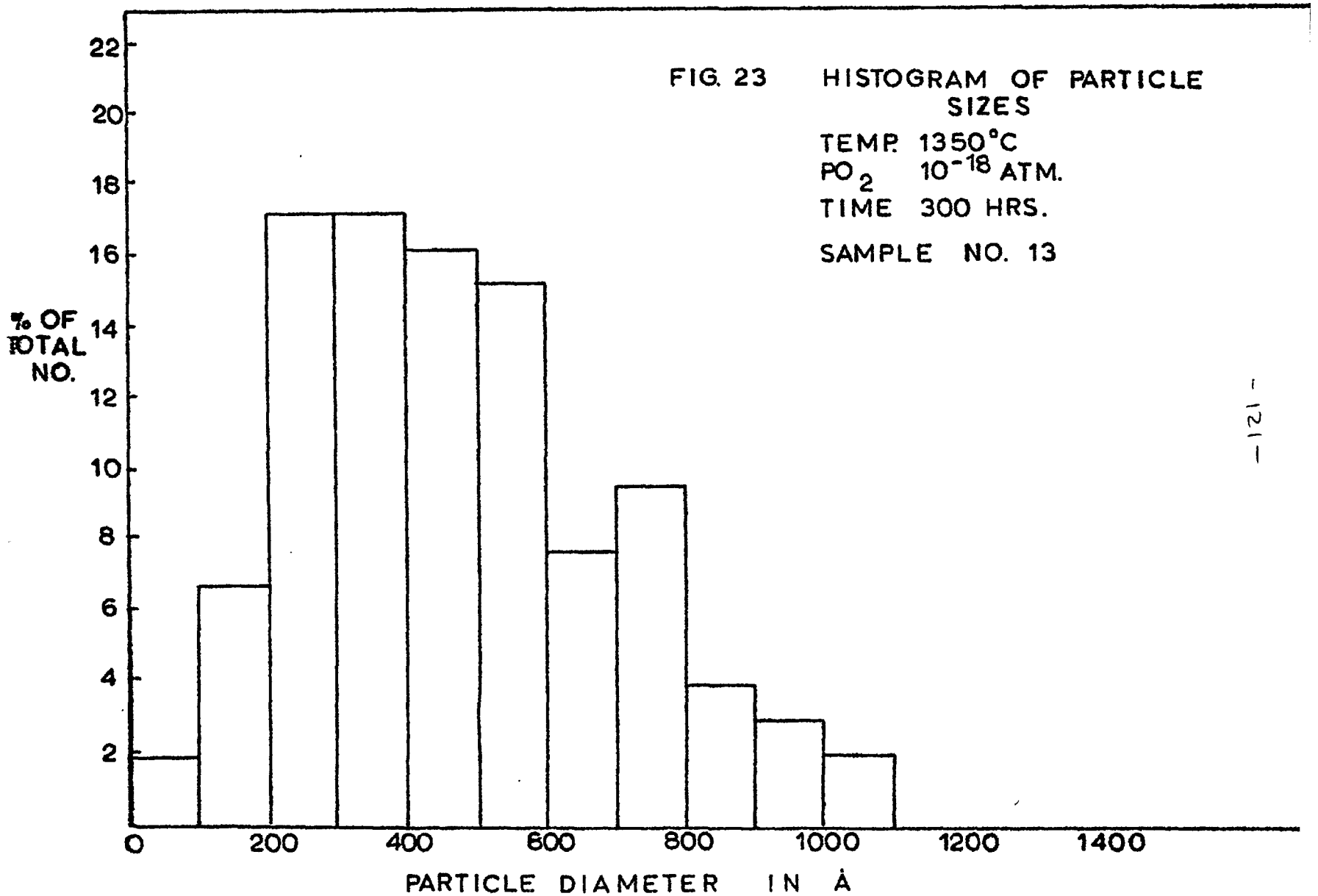

FIG. 23 HISTOGRAM OF PARTICLE SIZES

TEMP. 1350°C

PO_2 10^{-18} ATM.

TIME 300 HRS.

SAMPLE NO. 13

SAMPLE NO. 14 400 Hours at $PO_2 = 10^{-18}$ atm.

Diameter Interval (A)	No. Of Particles	% Of Total
0 - 50	0	0·00
50 - 100	0	0·00
100 - 150	6	4·08
150 - 200	6	4·08
200 - 250	9	6·12
250 - 300	5	3·63
300 - 350	13	9·53
350 - 400	12	8·16
400 - 450	3	2·04
450 - 500	14	10·31
500 - 550	10	7·25
550 - 600	3	2·04
600 - 650	2	1·45
650 - 700	4	2·90
700 - 750	9	6·12
750 - 800	6	4·08
800 - 850	6	4·08
850 - 900	5	3·63
900 - 950	4	2·90
950 - 1000	3	2·04
1000 - 1050	3	2·04
1050 - 1100	3	2·04
>1100	12	8·16
TOTAL NO.	138	

Mean radius = 299·6 A $\bar{r}^3 = 26{\cdot}90 \times 10^{18} cm^3$

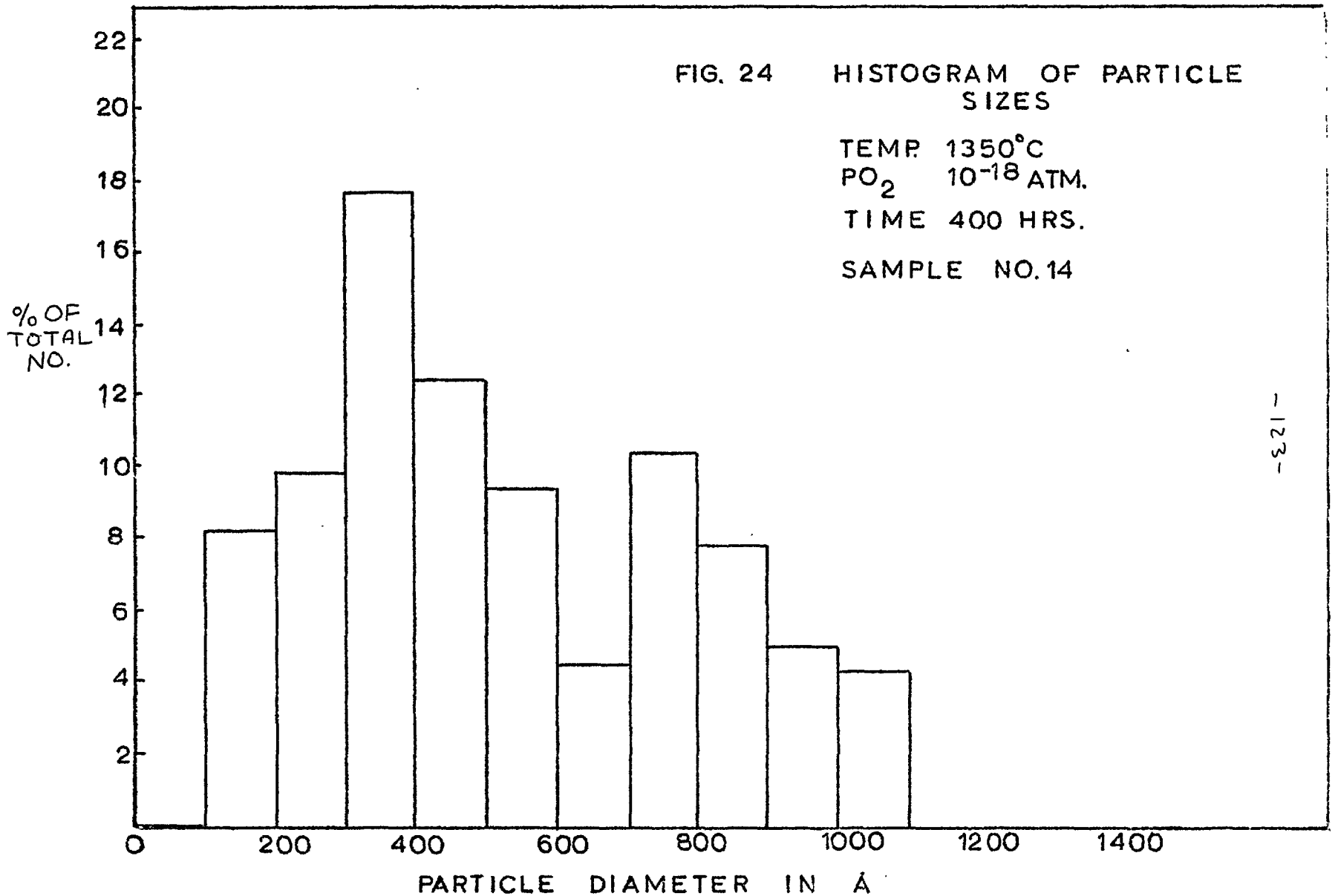
FIG. 24 HISTOGRAM OF PARTICLE SIZES
TEMP. 1350°C
PO_2 10^{-18} ATM.
TIME 400 HRS.
SAMPLE NO. 14
% OF TOTAL NO.
22
20
18
16
14
12
10
8
6
4
2
0
200
400
600
800
1000
1200
1400
PARTICLE DIAMETER IN Å

SAMPLE NO. 18 Pure Ni

$PO_2 = 10^{-18}$ Atm Anneal time = $14 \cdot 94 \times 10^4$ sec.

Channel No.	Channel Counts	t*	D $\times 10^{14}$ $cm^2 sec^{-1}$
6	9585	1·178	1·91
7	6965	1·283	1·84
8	4828	1·396	1·76
9	3393	1·499	1·76
10	2368	1·600	1·77
11	1783	1·676	1·86
12	1318	1·754	1·93
13	991	1·821	2·02
14	877	1·853	2·23
15	591	1·945	2·23
		Mean D	1·93

Regression Coefficient = 0·9917
Intercept = 0·7916
$Co/_2$ = 30960 counts
Sample Area = 2·28 cm^2
Counting time = 2 3·6 x 10^4 sec.
Co* = 0·262 counts sec^{-1}

Solubility = $9 \cdot 40 \times 10^{-2}$ Wt. %
Diffusion Coefficient = $1 \cdot 93 (\pm 0 \cdot 30) \times 10^{-14}$ $cm^2 sec^{-1}$

SAMPLE NO. 19 Pure Ni

$PO_2 = 10^{-18}$ Atm Annel time = $7\cdot92 \times 10^4$ sec.

Channel No.	Channel Counts	t*	D $\times 10^{14}$ $cm^2 sec^{-1}$
6	841	1·222	8·19
7	569	1·347	5·61
8	407	1·446	4·94
9	274	1·559	4·36
10	200	1·644	4·32
11	182	1·669	4·91
12	164	1·697	5·49
13	123	1·771	5·48
14	164	1·697	7·37
15	119	1·782	7·10
		Mean D	5·77

Regression Coefficient = 0·9335

Intercept = 0·9753

$Co/_2$ = 1678 counts

Sample Area = 2·28 cm^2

Counting time = $2\cdot49 \times 10^4$ sec

Co* = 0·135 counts sec^{-1}

Solubility = $4\cdot82 \times 10^{-2}$ Wt. %

Diffusion Coefficient = $5\cdot77 (\pm 1\cdot4) \times 10^{-14}$ $cm^2 sec^{-1}$

SAMPLE NO. 20 Ni 95% - Cr 5%

$PO_2 = 10^{-18}$ Atm. Anneal time = $6 \cdot 48 \times 10^4$ sec.

Channel No.	Channel Counts	t*	D $\times 10^{14}$ $cm^2 sec^{-1}$
6	3006	0·732	15·05
7	1535	1·010	5·01
8	1184	1·103	4·90
9	962	1·175	5·07
10	772	1·250	5·24
11	639	1·311	5·55
12	529	1·368	5·82
13	482	1·397	6·42
14	432	1·429	6·97
15	400	1·453	7·63
		Mean D	6·77

Regression Coefficient = 0·9377

Interceopt = 0·4888

$Co/_2$ = 4896

Sample Area = 1·90 cm^2

Counting time = $6 \cdot 0 \times 10^4$ sec

Co* = 0·163 counts sec^{-1}

Solubility = $6 \cdot 06 \times 10^{-2}$ Wt. %

Diffusion Coefficient = $6 \cdot 77 (\pm 9 \cdot 1) \times 10^{-14}$ $cm^2 sec^{-1}$

SAMPLE NO. 21 Ni 95% - Cr 5%

$PO_2 = 10^{-18}$ Atm. Anneal time = $14 \cdot 94 \times 10^4$ sec.

Channel No.	Channel Counts	t*	D $\times 10^{14}$ $cm^2 sec^{-1}$
6	1168	1·110	6·03
7	902	1·198	4·49
8	728	1·269	4·12
9	576	1·344	3·84
10	505	1·384	4·11
11	458	1·414	4·51
12	420	1·439	4·94
13	344	1·496	4·85
14	349	1·492	5·67
15	282	1·552	5·54
		Mean D	4·81

Regression Coefficient = 0·9747

Intercept = 0·8938

$Co/_2$ = 2060

Sample Area = 1·90 cm^2

Counting time = $6 \cdot 264 \times 10^4$ sec

Co* = $6 \cdot 58 \times 10^{-2}$ counts sec^{-1}

Solubility = $2 \cdot 44 \times 10^{-2}$ Wt. %

Diffusion Coefficient = $4 \cdot 81 (\pm 1 \cdot 20) \times 10^{-14}$ $cm^2 sec^{-1}$

SAMPLE NO. 22 Ni 95% - Cr 5%

$PO_2 = 10^{-18}$ Atm. Anneal time = $21{\cdot}42 \times 10^4$ sec.

Channel No.	Channel Counts	t*	D $\times 10^{14}$ $cm^2 sec^{-1}$
6	4707	0·511	3·77
7	3516	0·660	2·74
8	2659	0·788	2·38
9	2200	0·868	2·41
10	1746	0·959	2·38
11	1543	1·008	2·59
12	1262	1·082	2·63
13	1022	1·156	2·66
14	870	1·209	2·77
15	803	1·237	3·02
		Mean D	2·74

Regression Coefficient = 0·9817

Intercept = 0·1203

$Co/_2$ = 8650 counts

Sample Area = 1·9 cm^2

Counting time = $24{\cdot}27 \times 10^4$ sec

Co* = $7{\cdot}13 \times 10^2$ counts sec^{-1}

Solubility = $3{\cdot}06 \times 10^{-2}$ Wt. %

Diffusion Coefficient = $2{\cdot}74\ (\mp 1{\cdot}02) \times 10^{-14}$ $cm^2 sec^{-1}$

SAMPLE NO. 23 Ni 90% - Cr 10%

$PO_2 = 10^{-18}$ Atm. Anneal time = $7 \cdot 59 \times 10^4$ sec.

Channel No.	Channel Counts	t*	D $\times 10^{14}$ $cm^2 sec^{-1}$
6	391	1·464	3·97
7	281	1·556	3·74
8	225	1·612	4·02
9	161	1·704	3·92
10	110	1·796	3·83
11	85	1·863	4·04
12	53	1·973	3·86
13	62	1·938	4·82
14	50	1·987	5·07
15	34	2·072	4·99
		Mean D	4·23

Regression Coefficient = 0·9832

Intercept = 1·0966

$Co/_2$ = 1210 counts

Sample Area = 1·95 cm^2

Counting time = $2 \cdot 21 \times 10^4$ sec

Co* = 0·109 counts sec^{-1}

Solubility = $4 \cdot 58 \times 10^{-2}$ Wt. %

Diffusion Coefficient = $4 \cdot 32 (\mp 0 \cdot 49) \times 10^{-14}$ $cm^2 sec^{-1}$

SAMPLE NO. 24 Ni 90% - Cr 10%

$PO_2 = 10^{-18}$ Atm. Anneal time = $4 \cdot 61 \times 10^4$ sec.

Channel No.	Channel Counts	t*	D $\times 10^{14}$ $cm^2 sec^{-1}$
6	1179	1·107	13·68
7	958	1·178	12·46
8	702	1·280	10·46
9	562	1·351	10·38
10	466	1·407	10·75
11	380	1·469	11·02
12	374	1·471	12·90
13	288	1·546	12·50
14	293	1·542	10·56
15	224	1·612	14·15
		Mean D	12·28

Regression Coefficient = 0·9775

Intercept = 0·8330

$Co/_2$ = 2388 counts

Sample Area = 1·65 cm^2

Counting time = $2 \cdot 09 \times 10^4$ sec

Co* = 0·229 counts sec^{-1}

Solubility = $11 \cdot 30 \times 10^{-2}$ Wt. %

Diffusion Coefficient = $12 \cdot 28 (\mp 2 \cdot 28) \times 10^{14}$ $cm^2 sec^{-1}$

SAMPLE NO. 25 Ni 90% - Cr 10%

$PO_2 = 10^{-18}$ Atm. Anneal time = $12{\cdot}77 \times 10^4$ sec

Channel No.	Channel Counts	t*	D $\times 10^{14}$ $cm^2 sec^{-1}$
6	2249	0·859	4·35
7	1653	0·981	3·51
8	1194	1·103	3·12
9	943	1·187	3·10
10	742	1·262	3·20
11	632	1·315	3·45
12	514	1·369	3·58
13	429	1·433	3·76
14	350	1·492	3·89
15	322	1·513	4·27
		Mean D	3·62

Regression Coefficient = 0·9825

Intercept = 0·4796

$Co/_2$ = 4834

Sample Area = 1·65 cm^2

Counting time = $10{\cdot}8 \times 10^4$ sec

Co* = $4{\cdot}47 \times 10^{-1}$ counts sec^{-1}

Solubility = $4{\cdot}42 \times 10^{-2}$ Wt. %

Diffusion Coefficient = $3{\cdot}62\ (\mp 0{\cdot}73) \times 10^{-14}$ $cm^2 sec^{-1}$

SAMPLE NO. 26 Ni 85% - Cr 15%

$PO_2 = 10^{-18}$ Atm. Anneal time = $7 \cdot 59 \times 10^4$ sec.

Channel No.	Channel Counts	t*	D $\times 10^{14}$ $cm^2 sec^{-1}$
6	1127	1·121	3·90
7	833	1·225	3·77
8	641	1·310	3·90
9	447	1·421	3·78
10	337	1·503	3·92
11	218	1·625	3·78
12	150	1·718	3·81
13	141	1·736	4·32
14	99	1·824	4·36
15	94	1·839	4·90
		Mean D	4·05

Regression Coefficient = 0·9888

Intercept = 0·6536

$C_{o/2}$ = 3554 counts

Sample Area = 1·86 cm^2

Counting time = $6 \cdot 51 \times 10^4$ sec

Co* = $1 \cdot 09 \times 10^{-1}$ counts sec^{-1}

Solubility = $4 \cdot 79 \times 10^{-2}$ Wt.%

Diffusion Coefficient = $4 \cdot 05 (\mp 0 \cdot 81) \times 10^{-14}$ $cm^2 sec^{-1}$

SAMPLE NO. 27 Ni 85% - Cr 15%

$PO_2 = 10^{-18}$ Atm. Anneal time = $7{\cdot}38 \times 10^4$ sec.

Channel No.	Channel Counts	t*	D $\times 10^{-14}$ $cm^2 sec^{-1}$
6	1684	0·972	19·02
7	1223	1·092	10·44
8	959	1·178	8·89
9	801	1·237	8·75
10	791	1·242	10·71
11	687	1·289	10·94
12	594	1·333	11·11
13	569	1·347	12·46
14	524	1·372	13·25
15	463	1·411	13·74
		Mean D	11·93

Regression Coefficient = 0·9572

Intercept = 0·7969

$Co/_2$ = 2601 counts

Sample Area = 1·8 cm^2

Counting time = $6{\cdot}57 \times 10^4$ sec.

Co* = $7{\cdot}92 \times 10^{-2}$ counts scc^{-1}

Solubility = $3{\cdot}58 \times 10^{-2}$ Wt. %

Diffusion Coefficient = 11·93 ($\mp$3·2) $\times 10^{-14}$ $cm^2 sec^{-1}$

SAMPLE NO. 28 Ni 85% - Cr 15%

$PO_2 = 10^{-18}$ Atm. Anneal time = $10{\cdot}71 \times 10^4$ sec.

Channel No.	Channel Counts	t*	D $\times 10^{14}$ $cm^2 sec^{-1}$
6	2205	0·866	6·40
7	1691	0·972	5·16
8	1356	1·056	4·91
9	1080	1·135	4·73
10	572	1·209	4·75
11	780	1·246	5·22
12	678	1·292	5·55
13	546	1·358	5·55
14	478	1·398	5·88
15	429	1·432	6·28
		Mean D	5·44

Regression Coefficient = 0·9869

Intercept = 0·5549

$Co/_2$ = 4324 counts

Sample Area = 1·8 cm^2

Counting time = $8{\cdot}64 \times 10^4$ sec.

Co* = 0·10 counts sec^{-1}

Solubility = $4{\cdot}54 \times 10^{-2}$ Wt. %

Diffusion Coefficient = $5{\cdot}44\ (\mp 1{\cdot}00) \times 10^{14}$ $cm^2 sec^{-1}$

SAMPLE NO. 29 Ni 80% - Cr 20%

$PO_2 = 10^{-18}$ Atm. Anneal time = $7 \cdot 16 \times 10^4$ sec.

Channel No.	Channel Counts	t*	D $\times 10^{14}$ $cm^2 sec^{-1}$
6	470	1·404	5·51
7	278	1·556	5·90
8	203	1·641	3·90
9	150	1·718	3·96
10	98	1·824	3·81
11	104	1·810	4·74
12	95	1·839	5·37
13	65	1·930	6·25
14	57	1·959	5·68
15	32	2·079	5·19
		Mean D	5·03

Regression Coefficient = 0·9741

Intercept = 1·095

Co/2 = 1214 counts

Sample Area = 2·01 cm^2

Counting time = $2 \cdot 46 \times 10^4$ sec.

Co* = $9 \cdot 86 \times 10^{-2}$ counts sec^{-1}

Solubility = $4 \cdot 00 \times 10^{-2}$ Wt. %

Diffusion Coefficient = $5 \cdot 03 (\mp 1 \cdot 22) \times 10^{-14}$ $cm^2 sec^{-1}$

REFERENCES

1. Wood, D.L. Trans. A.I.M.E. 215 (1959) 925.
2. Butterd, A. Zwilsky, K. Grant, N. Trans. A.S.M. 56 (1963) 509
3. Smith, C.G. Powder Met. 11 (1963) 102.
4. Mitchell, J. Mitra, S. Dorn, J. Trans. A.S.M. 56 (1963) 237.
5. Gregory, C. Goetzel, C. Trans. A.I.M.E. 212 (1958) 868.
6. White, J.E. Powder Met. 8 (No. 15) (1965) 64.
7. Bonis, L. Grant, N. Trans. A.I.M.E. 224 (1962) 308.
8. Seybolt, A. Trans. A.S.M. 59 (1966) 860.
9. Rassmussen, J. Grant, N. Powder Met. 8 (1961) 92.
10. Grimwade, M. G.E.C. Report ISMET 3755 HR 739.
11. Cremens, W. Grant, N. Proc. A.S.M. 58 (1958) 714.
12. Wilcox, B. Clauer, A. McCain, W. Trans. A.I.M.E. 239 (1967) 1791.
13. Zwilsky, K. Grant, N. Trans. A.I.M.E. 209 (1957) 1197.
14. White, J. Carnahan, R. Trans. A.I.M.E. 230 (1964) 1298.
15. Martin, J. Smith, C.G. J. Inst. Metals 83 (1954) 417.

16. King, G. Sell, H. Trans. A.I.M.E. 233 (1965) 1104.

17. Hiltz, R. Grant, N. Trans. A.I.M.E. 212 (1958) 383.

18. Gregory, C. Smith, G.C. J. Inst. Metals 85 (1956) 81.

19. Ansell, G. Kim, H. Powder Met. 10 (1962) 52.

20. Goodrich, R. Ansell, G. Acta. Met. 12 (1964) 1097.

21. Von Heimendahl, M. Thomas, G. Trans. A.I.M.E. 230 (1964) 1520.

22. Doble, G. Quigg, R. Trans. A.I.M.E. 233 (1965) 410.

23. Greenwood, G. Acta. Met. 4 (1956) 243.

24. Lifshitz, I. Slyozov, V. J. Ph. Ch. Solids 19 (1961) 35.

25. Wagner, C. Z.Electro. Chem. 65 (1961) 581.

26. Heckel, R. Trans. A.I.M.E. 233 (1965) 1994.

27. Brown, P. Ph.D. Thesis London (1967)

28. Livingston, J. Trans. A.I.M.E. 215 (1959) 566.

29. Heckel, R. DeGregorio, R. Trans. A.I.M.E. 233 (1965) 2001.

30. Smith, A.F. Acta. Met. 15 (1967) 1867.

31. Smith, A.F. J. Less. Com. Metals. 9 (1965) 233.

32. Speich, G. Oriani, R. Trans. A.I.M.E. 233 (1965) 623.

33. Ardell, A. Nicholson, R. J. Ph.Ch. Solids 27 (1966) 1793.

34. Sims, C.T. Trans. A.I.M.E. 227 (1963) 1455.

35. Servi, I. Turnbull D. Acta. Met. 14 (1966) 161.

36. Murphy R. Grant, N. Powder Met. 10 (1962) 1.

37. Grimwade, M. Jackson, K. Powder Met. 10 (1962) 13.

38. Tracey, V. Worn, D. Powder Met. 10 (1962) 34.

39. Gatti, A. Powder Met. 10 (1962) 77.

40. Lewis, M. Seebohm, R. Martin, J. Powder Met. 10 (1962) 87.

41. Feisel, D. Cochardt, A. Trans. A.I.M.E. 215 (1959) 608.

42. Inman, M. Smith, P.J. "Department of Commerce Clearinghouse Report" (1966(, A.D.- 636487.

43. Komatsu, N. Grant, N. Trans. A.I.M.E. 224 (1962) 705.

44. Dromsky, J. Lenel, F. Ansell, G. Trans. A.I.M.E. 224 (1962) 236.

45. Sergeenkova, Miss V. Beresutskii, V. Sov. Powder Met. Metall. Ceram. 8 (1967,) 640.

46. Humenick, M. Kingery, W. J.Am. Ceram. Soc. 37 (1954) 18.

47. Armstrong, W. Chacklader, A. Clarke, J. J.Am. Ceram. Soc. 45 (1962) 115.

48. Udin, H. Wulff, J. J. Metals 3 (1951) 1206.

49. Seitz, F. "The Physics of Metals" McGraw-Hill (1943).

ACKNOWLEDGEMENTS

The author would like to thank his supervisor, Professor C. B. Alcock, for providing the research facilities and giving useful advice on the research project. Thanks are also extended to all members of the Nuffield Research Group for their assistance and useful discussions.

The author would also like to express his gratitude to the Ministry of Technology for providing the financial support for this research project.